AFRL-AFOSR-VA-TR-2020-0112

Structure-Photophysics-Function Relationship of Perovskite Materials

He Wang
UNIVERSITY OF MIAMI

07/15/2020
Final Report

Air Force Research Laboratory
AF Office Of Scientific Research (AFOSR)/ RTB2
Arlington, Virginia 22203
Air Force Materiel Command

DISTRIBUTION A: Distribution approved for public release.

REPORT DOCUMENTATION PAGE

Form Approved
OMB No. 0704-0188

1. REPORT DATE *(DD-MM-YYYY)*	2. REPORT TYPE	3. DATES COVERED *(From - To)*
22-07-2020	Final Performance	15 Apr 2017 to 14 Apr 2020

4. TITLE AND SUBTITLE
Structure-Photophysics-Function Relationship of Perovskite Materials

5a. CONTRACT NUMBER

5b. GRANT NUMBER
FA9550-17-1-0099

5c. PROGRAM ELEMENT NUMBER
61102F

6. AUTHOR(S)
He Wang

5d. PROJECT NUMBER

5e. TASK NUMBER

5f. WORK UNIT NUMBER

7. PERFORMING ORGANIZATION NAME(S) AND ADDRESS(ES)
UNIVERSITY OF MIAMI
1551 BRECIA AVE RM 100A
CORAL GABLES, FL 331462503 US

8. PERFORMING ORGANIZATION REPORT NUMBER

9. SPONSORING/MONITORING AGENCY NAME(S) AND ADDRESS(ES)
AF Office of Scientific Research
875 N. Randolph St. Room 3112
Arlington, VA 22203

10. SPONSOR/MONITOR'S ACRONYM(S)
AFRL/AFOSR RTB2

11. SPONSOR/MONITOR'S REPORT NUMBER(S)
AFRL-AFOSR-VA-TR-2020-0112

12. DISTRIBUTION/AVAILABILITY STATEMENT
A DISTRIBUTION UNLIMITED: PB Public Release

13. SUPPLEMENTARY NOTES

14. ABSTRACT
Organometal halides that adopt perovskite structure have received tremendous attention due to the rapid increase in power conversion efficiency of solar cells. The perovskite film is sensitive to subtle variations during the fabrication. Characterizing the structure and testing the device performance only probes its static properties. Converting from photon to separated electron and hole is a dynamic process ranging from femtosecond to microsecond. Ultrafast laser spectroscopy can be utilized to study photophysics, but photophysics of different films has not been well correlated with structure and device function. In order to better understand the structure-function relationship, the uniqueness of our direction is to use femtosecond laser spectroscopy to study photophysics of different structures. This project focuses on studying the structure, photophysics, and function for a series of organic-inorganic hybrid perovskite materials and structures, which can be useful

15. SUBJECT TERMS
hybrid perovskite materials, photophysics, structure properties relationship, materials morphology

16. SECURITY CLASSIFICATION OF:			17. LIMITATION OF ABSTRACT	18. NUMBER OF PAGES	19a. NAME OF RESPONSIBLE PERSON
a. REPORT	b. ABSTRACT	c. THIS PAGE			CASTER, KENNETH
Unclassified	Unclassified	Unclassified	UU		19b. TELEPHONE NUMBER *(Include area code)* 703-588-8487

Standard Form 298 (Rev. 8/98)
Prescribed by ANSI Std. Z39.18

Final Report for AFOSR Grant FA9550-17-1-0099 "Structure-Photophysics-Function Relationship of Perovskite Materials"

July 13, 2020

PI information:
Name of Principal Investigator: He Wang
e-mail address: hewang@miami.edu
Institution: University of Miami
Department: Physics
Mailing Address: 1320 Campo Sano Ave, Coral Gables, 33146, FL, USA
Phone: 305-284-7126
Fax: 305-284-4222

Period of Performance: 04/15/2017 - 04/14/2020

Abstract: Organometal halides that adopt perovskite structure have received tremendous attention due to the rapid increase in power conversion efficiency of solar cells. The perovskite film is sensitive to subtle variations during the fabrication. Characterizing the structure and testing the device performance only probes its static properties. Converting from photon to separated electron and hole is a dynamic process ranging from femtosecond to microsecond. Ultrafast laser spectroscopy can be utilized to study photophysics, but photophysics of different films has not been well correlated with structure and device function. In order to better understand the structure-function relatio nship, the uniqueness of our direction is to use femtosecond laser spectroscopy to study photophysics of different structures. This project focuses on studying the structure , photophysics , and function for a series of organic-inorganic hybrid perovskite materials and structures , which can be useful design motif on the choice of materials and structures for their device application.

We have completed our goals. We studied structure-photophysics-function relationship of quasi-2D perovskite solar cells, using large-size organic cation to improve stability and efficiency of perovskite solar cells, age-induced recrystallizat io n, and the effect of reactant in the formation of perovskite. In addition, we utilized transient absorption and reflection spectroscopy to understand the carrier spin lifetime , charge transfer and diffusion at the inter face, and coherent phonon. It also offers an excellent platform for the collaboration with other research groups on photophysics of different organic and hybrid materials. With the AFOSR YIP support ($360,000), we published 10 papers in 3 years, out of which six as corresponding author and four as co-author. We also have one co-authored paper submitted and one (corresponding author) in preparation.

1. Introduction:

Organometal halides that adopt perovskite structure have received tremendous attention due to the rapid increase in power conversion efficiency of solar cells.[1,2] This stems from its unique optoelectronic properties, including broad absorption,[2-3] weak exciton binding energy,[4-6] ambipolar charge transport,[7-10] and limited electron-hole recombination.[3, 10-14] It has not been clear how microstructures affect free carrier dynamics macroscopically, with a priori prediction of device performance based on structure not yet possible. This project focuses on studying the structure, photophysics, and function for a series of organic-inorganic hybrid perovskite materials and structures, which can be useful design motif on the choice of materials and structures for their device application.

The perovskite film is sensitive to subtle variations during the fabrication. Characterizing the structure and testing the device performance only probes its static properties. Converting from photon to separated electron and hole is a dynamic process ranging from femtosecond to microsecond. A priori prediction of device properties based on structure is not yet available. Ultrafast laser spectroscopy can be utilized to study photophysics, but photophysics of different films has not been well correlated with structure and device function. It is not straightforward to build this correlation, since it requires the abilities of performing all the aspect experiments, including materials characterization, device, and laser spectroscopy. My interdisciplinary research experiences allow me to quickly develop an independent research group by leveraging the abilities of ultrafast laser spectroscopy, materials characterization, and device physics. **A key feature of my research is to build a photophysics bridge to better connect structure and optoelectronic properties. (Figure 1)** Although the field is highly competitive and fast moving, to the best of my knowledge, our approach is a unique and promising one.

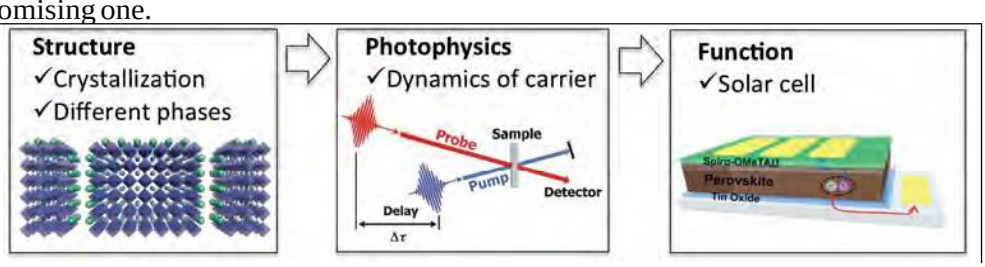

Figure 1. Structure-photophysics-function relationship of perovskite solar cells.

We have studied phase distribution of quasi-2D perovskite solar cells, improving stability and efficiency of perovskite solar cells using large-size organic cation, age-induced perovskite recrystallization, and the effect of reactant in the formation of perovskite (see section 1.1). Besides studying the fundamental mechanism in hybrid perovskite solar cells, we utilized transient absorption and reflection spectroscopy to understand the carrier spin lifetime, charge transfer and diffusion at the interface, and coherent phonon (see section 1.2). In addition to structure-photophysics-function relationship of perovskite materials, we also utilize our expertise of ultrafast laser spectroscopy to collaborate with other groups to study photophysics of perovskites, organic semiconductors, and organic ligand protected metal nanoclusters (see section 1.3).

With the AFOSR YIP support ($360,000), we published 10 papers in 3 years, out of which six as corresponding author and four as co-author. We also have one co-authored paper submitted and one (corresponding author) in preparation.

1.1 Structure-photophysics-function relationship of hybrid perovskite solar cells

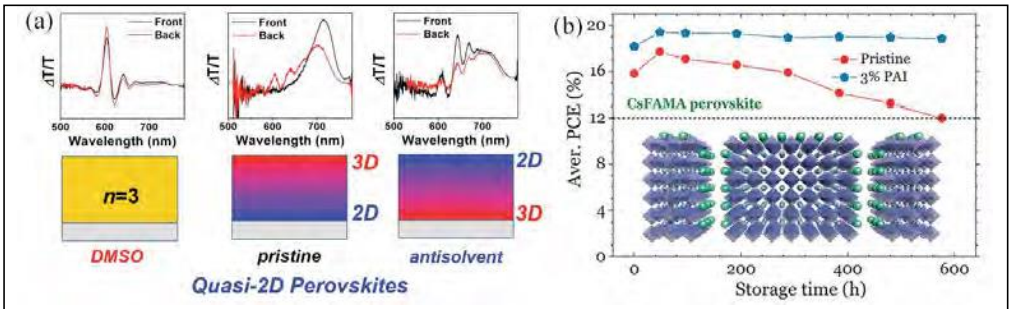

Figure 2. (a) Transient absorption spectra of three quasi-2D perovskite films with different phase purities and vertical distributions from Ref [15] (b) Perovskite solar cell device performance and stability (pristine and those treated by large-size organic cation) from Ref [16] .

1) Introducing large size hydrophobic cation (such as butylammonium , BA) into 3D perovskite (CH_3NH_3Pbb , MAPbb) to create quasi-2D perovskite can improve device stability. It is challenging to control and characterize the composition and structure. We manipulated the phase purity and vertical distribution of quasi-2D perovskite proven by ultrafast transient absorption spectroscopy with front and back laser exc itation. [15] ***(Solar RRL,*** *2019, 3, 1800359, selected by Wiley hot topic: solar cells)* We found that solar cell performance is more sensitive to phase purity relative to vertical distribution . **(Figure 2a)**

2) Introducing a small amount of large size hydrophobic cation into a 3D perovskite structure without interrupting the crystal structure is a promising method for maintaining high effic ie ncy, while enhancing its stability against moisture. By comparing a family of different cations, our results show that propylammonium (PA) cation is the most effective one at mitigating these instability issues. Via femtosecond transient absorption and reflection spectroscopy, we found that the large cations preferentially accumulate at the grain boundaries and film surfaces.[16] ***(J. Mater. Chem. A,*** 2019, 7, 23739, ***2019 Emerging Investigator Themed Issue)*** The preferential crystal orie ntation, crysta llization, and grain size in both lateral and vertical directions are enhanced accordingly. Such self-assembled large cations suppress the charge recombination and enhance device efficiency to 20.1%. Along with improvements in efficiency, the addition of the PA cation significantly improves both device and precursor stabilities. The efficiency of pristine perovskite decreases by 32.1%, while those with PA only decrease by 2.8% after 600 hours under low and/or high humidity. **(Figure 2b)**

3) The highest efficiency (20.1%) usually appears some time after the device fabrication. We utilize X-ray diffraction, time-resolved photoluminescence, transient absorption spectrometer, and single-carrier diode measurement to understand the structure and electronic properties. We observe enhanced crystallinity and crystallite size, referred to as age-induced recrystallization. Based on the structural changes, the charge trap and recombination are suppressed, while charge transport and collection are enhanced, ultimately improving device efficiency.[17] ***(Org. Electron.,*** 2019, 68, 143).

4) The black phase of inorganic perovskite CsPbh is extremely unstable at room temperature. The difficulty stems from the lack of effective approaches to maintain the black phase in functional device and insufficient understanding of its reactant dimethylammonium lead iodide ($DMAPbI_3$). By tuning the time and temperature, powder

and crystal DMAPbb are synthesized. Interest ingly , the good-looking DMAPbh crystal is a mixture of multiple phases (hexagonal and trigo nal), gradual growth from unstable small bandgap structure in the center outwards to stable large bandgap face-sharing of PbI6 oc tahed ra. The CsPbb films fabricated from crystal DMAPbh display higher crystallinity and larger grain size, enhancing both phase and photo stabi lity , and improving solar cell efficiency to 18.07%. (manuscript in preparation)

1.2 Photophysics of perovskite materials

5) Besides solar cells, lead halide perovskites are promising candidates in spintronics. We utilized circular polarized transient absorption spectroscopy to quantify spin lifetime of perovskite with different compositions.[18] **(J. *Phys. Chem. Lett.*,** 2020, 11, 1502) We find that molar mass plays a dominant role of spin orbital coupling in their spin relaxation. It is suggested that two different mechanisms , namely Elliot-Yafet in which spin flips upon momentum scattering , and D'yakonov-Perel in which spin relaxes between momentum scattering, are responsible for spin relaxation of perovskite with different compositions. Our work for the first time illustrates the effect of composition on the spin relaxation and mechanism of perovskites and will stimulate future research on spin dynamics and spintronic devices.

6) Transient absorption and reflection spectroscopy were utilized to probe the ultrafast charge diffusion in perovskite film and charge transfer from perovskite to an adjacent electron transport layer.[19] **(J. *Phys. Chem.* C,** 2019, 123, 22095) A sub-picosecond charge transfer coupled with carrier diffusion and hot carrier cooling is observed. We find that more significant surface recombination in perovskite films caused by pinholes competes with interfacial charge transfer, which lowers charge transfer efficiency.

7) We utilized temperature-, fluence-, and polarization-dependent transient absorption spectroscopy to study coherent phonon in perovskite , which refers to the in-phase vibration of crystal lattice.[20] **(J. *Phys. Chem.* C,** 2018, 122, 17035) The generation mechanism of coherent phonon is impulsive stimulated raman scattering and transient depletion field screening.

1.3 Photophysics of perovskite and other organic materials via collaboration

We utilized our expertise of ultrafast laser spectroscopy to collaborate with other groups to study photophysics of perovskites, organic semiconduc tors, and organic ligand protected metal nanocluste rs.

8) We collaborated with Prof. Zhibin Yu at Florida State University, AFOSR YIP recipient in the Or anic Materials Chemistry Divisio n, on a rous halide perovskite–polymer nanocomposite *A dv. Mater. Inter.*, 2019, 6, **180168611fhe** trans ie nt absorption spectroscopy probes the traps and charge transfer that contribute to fluorescence quenching of perovskite caused by the polymer nanocomposite. [21]

9) We collaborated with Prof. Rongchao Jin at Carnegie Mellon University, a world leading group in the synthesis of hybrid nanoc l usters , to study photophysics in organic ligand protected metal nanoclusters. Femtosecond pump-probe experiment s were performed to understand the charge transfer behaviors in different organic ligand protected metal nanoclusters. One paper was published *(ACS Nano,* 2020, 14, 6599) [22] and the other was recently submitted.

10) I am collaborating with Prof. Zenghu Chang at University of Central Flo rida, a leading group in attosecond science in the world. His research has been strongly suppo rted by DoD including AFOSR, ARO, and ONR. Our collaboration aims to study charge transfer

in organic semiconductors via femtosecond and attosecond transient absorption spectroscopy. Our perspective, with a section on probing charge transfer in organ ic li ght harvesting systems via attosecond transient absorption spectroscopy, is recently published in *Nature Communications (Nat. Commun.,* 2020, 11, 2748).[23] This takes advantage of the lates t developme nt of attosecond soft X-ray so urces in the " Wate r Window" (282 to 533 eV) in Chang' s group that can probe the C, N, and Ti edges. It also leverages my interdisciplinary experiences in organic solar cells, femtosecond laser spectroscopy , and synchrotron based soft X-rays.

11) We collaborated with Prof. Hebin Li at Florida International Unive rsity, an expert on 2D electronic spectroscopy, a process probing the coherent phonon and charge transfer between different electronic energy states in perovskite *(J Phys. Chem. Lett.,* 2019, 10, 4625. Journal Cover).[24]

12) Besides the above collaboration that has already published journal papers, we are also utilizing femtosecond laser spectroscopy to collaborate with others scientists. For example, we collaborated with Prof. Hanwei Gao at Florida State University, an ONR YIP rec ipie nt, to study carrier lifetime of different perovskites for light-emitting diode application. We ran transient absorption experiments to quantify spin lifetime of perovskite films fabricated by Prof. Stephanie Lee at Steven Institute of Technology and spin lifetime of graphene made by Prof. Xian Zhang at the same university.

2. Experiments: The details of experiment, equipment or analyses are described in the papers. Brie fly, the techniques include:

- Crystal structure , crysta llini ty, and grain size: We used X-ray diffraction (XRD) to characterize struct ure, crystallinity and crystallite size. [16] [17] To provide a conclusive determination of the crystal preferential orientation with respect to the substrate, we utilized grazing-incidence wide-angle X-ray scattering (GIWAXS) in Synchrotron Source.[16] Domain size from top view and cross-section view was observed with scanning electronic microscopy (SEM).[16]
- Carrier dynamics at the surface and in the bulk: We have established well-equipped ultrafast spectroscopy. Femtosecond transient absorption (TA) and transient reflection (TR) experiments were performed to study charge carrier dynamics in the bulk and at the sur face, respectively , from femtosecond to microsecond, and from visible to near infrared .[19] Time correlated single photon counting (TCSPC) was used to characterize time-resolved PL. [16] [17]
- Electronic characteristics: Trap density and carrier mobility was extracted by fabricating single-carrier diode and measuring the space-charge-limited current of electron-only and hole-only devices. [17] The type of traps (trap-assisted recombination and electron-hole recombination) were identified and recombination resistance was extracted.[16]
- Device: Efficiency of hybrid perovskite solar cell over 20% was reached in my lab. [16] [17]
- Calculation: Carrier dynamics and distribution along the film depth is calculated according to carrier diffusion, surface and bulk recombination, and charge transfer rate.[19] Exciton binding energy was extracted by fitting the absorption spectra to Elliott's formula. [18] These home-written Matlab codes are user-friendly.

3. Results and Discussion

Below describes the key results of seven sub-projects led by the PI's group. More details are in the published papers.

3.1 Manipulating Phase Distribution and Carrier Transfer in Quasi-2D Perovskites

Quasi-2D perovskites are promising alternatives to conventional 3D perovskites because of their high stability and easy tunability. However, controlling the phase distribution according to device architecture remains a major challenge. Here, we report the manipulation of phase purity and vertical distribution proved by ultrafast transient absorption spectroscopy, and their effect on device characteristics. By adding ethyl acetate as antisolvent, we flip the growth direction of perovskite film. CH_3NH_3Cl (MACl) and dimethyl sulfoxide (DMSO) are used to slow the growth rate of the crystal, which gives better phase purity. The direction of carrier migration is tuned accordingly. We find that solar cell performance is more sensitive to phase purity relative to vertical distribution. These findings are of importance for the applications of quasi-2D perovskites in different type of devices that require to change phase purity and vertical distribution. *(Solar RRL, 2019, 3, 1800359)*

3.1.1 Vertical phase distribution of pristine perovskite and that treated by antisolvent

Ultrafast transient absorption (TA) spectroscopy was performed to probe the carrier dynamics of films prepared under different conditions. In order to probe the vertical distribution , the laser excites the film in two different geometries, from the front (surface of the perovskite film) and from the back (substrate). First, we probed the pristine sample **(Figure 3).** In the transient absorption spectra (L'.1T/T) , positive signals correspond to ground state bleaching (GSB). With front excita tion , we can observe that *n=oo* GSB dominated the TA spectra while GSBs of lower-n are much weaker **(Figure 3a, b**). In contrast , with back excitation , GSBs of lower-n *(n=2*, 3, 4, 5) become significantly stronger while GSB of *n=oo* is weaker (Figure 5d, e). It suggests that in pristine film, 3D component is preferentially segregated on the surface while 2D components are preferentially accumulated at the bottom. Under both front and back excitation conditions , in less than 1 ps, the GSB peaks of smaller *n* decays to zero while the GSB of *n=oo* rises at the same time **(Figure 3c, f).** These features indicate electron or energy transfer from lower-n to *n=oo* in the film.

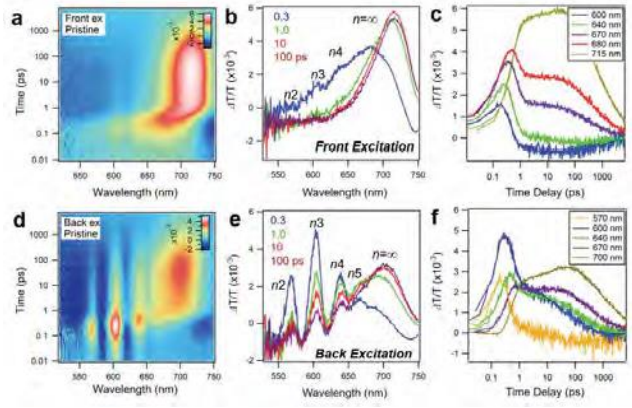

Figure 3. Carrier dynamics of pristine quasi-2D perovskites. TA (AT /T) data map , TA spectra at different time delays, kinetic traces and fitting at selected wavelength with (a-c) front excitation and with (d-f) back excitation.

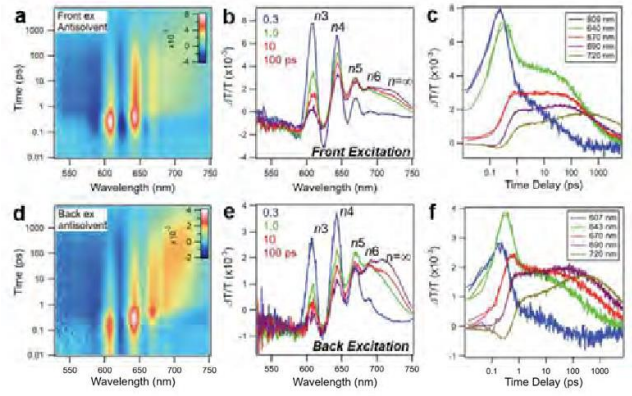

Figure 4. Carrier dynamics of quasi-2D perovskites after adding antisolvent. TA (i1T/T) data map , TA spectra at different time de lays, kinetic traces and fitting at selected wavelength with (a-c) front excitation and with (d-f) back excitation.

Antisolvent has been an effective method to enhance the crystallization of 3D perovskite, however, the effect of antisolvent on the vertical distribution in quasi-2D RPP is lack of understanding . Under both excitation cond it ions , one can observe GSBs corresponding to *n=3,* 4, 5, 6 while that of *n=2* is weakened **(Figure 4).** With front excitation, lower-n GSB peaks are stronger and those peaks are gradually weakened as n increases **(Figure 4a, b**). On the other hand, with back excitati on, GSBs at *n=3,* 4 are weaker while GSB with higher-n remains almost the same **(Figure 4d, e).** Therefore, the relative intensity of GSB at *n=oo* is much stronger with back excitation. All these spectral features suggest that after adding antisolvent, 2D component tends to segregate on the surface and 3D component tends to accumulate at the bottom.

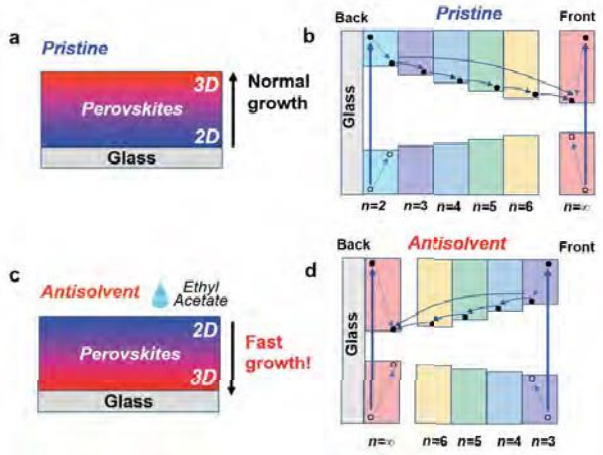

Figure 5. Schematic band structure and film distribution of $BA_2MA_3Pb_4I_{13}$ perovskite films with and without antisolvent. Film growth direction of (a) pristine sample and (c) sample adding antisolvent; band structure of (b) pristine film and (d) film adding antisolvent.

Based on the observation discussed above, the phase distribution and band structure of pristine film and film after adding antisolvent can be summarized in **Figure 5.** In pristine fi lms, the perovskite crystal growth is slow and lower-n phases grow first at the bottom and then higher-n phases at the top **(Figure Sa).** After adding antiso lvent , the perovskite crystal growth occurs quickly. Antisolvent is dropped from the top, so the surface of the film in contact with the antisolvent starts to crystallize first, which leads to lower-n phase segregated at the surface **(Figure Sc).**

3.1.2 Impact of MAC! and DMSO on phase purity

Knowing that antisolvent can flip the growth direction and the carrier migrations of quasi-2D perovskite film, we then sought to further control the phase distribution by modifying the fabrication process, in pursuit of pure phase. MACl has been used to slow down the crystallization rate via forming the intermediate state and increase the quality of 3D MAPbh perovskite film. [25] After adding MACI into quasi-2D perovskite, only GSB peaks for *n=3,* 4, 5 and a very weak peak for *n=oo* can be observed while those of other phases disappeared **(Figure 6a, b**). Moreover,

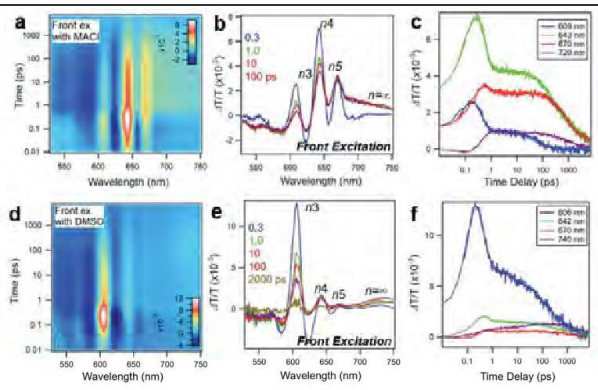

Figure 6. Carrier dynamics of quasi-2D perovskites after adding MAC! and DMSO. TA (L'.IT/T) data map, TA spectra at different time delays , kinetic traces and fitting at selected wavelength with addition of (a-c) MAC! and (d-t) DMSO at front excitation.

GSB peak for *n=4* is the most prominent, which indicates the addition of MAC! increases the phase towards larger *n* and the distribution is narrowed. With front and back excitations, there is no significant difference in TA spectra, which agrees with the fact that the phase distribution is narrowed **(Figure 6a, b**).

Mixed solvent (mixture of dimethylformamide (DMF) and DMSO) has also been used to modify the perovskite film quality by forming DMSO-Pbl 2 comp le x,[26] since DMSO has high affinity with the metal halide. [27] In the pursuit of single phase, we added DMSO as co-solvent. After using DMSO-DMF as co-solvent during the fabrication, GSB peak for *n=3* dominated the TA spectra while GSBs of other phases were much weaker **(Figure 6d, e).** All the absorption peaks are sharpened compared to those of the pristine film , which indicates better crystal quality.

Based on the above results, we then discuss how the crystal growth rate affects the phase distribution. As reported previo usly, [25] by introducing MAC! during the preparation of MAPbh, the reaction between CH3NH3I and Pblz is retarded by forming an intermediate product (CH3NH3PblzCI). Similar process is expected to occur in quasi-2D perovskite, thus the crystal growth process becomes slow and the nucleation rate is also reduced, which give rise to large crystallites and narrow phase distribution. The increase in the *n=4* phase after adding MAC! indicates narrowed phase distribution and further verifies the good quality of the film. DMSO has a higher boiling point than DMF, thus the evaporation rate of DMSO would be slower, increasing the grain size of the film.[27] As expected, the phase distribution is further narrowed and *n=3* phase dominates **(Figure 7b).** When the solvent evaporates slow ly, the crystal growth becomes slow and a larger grain size of perovskite can be formed. Here, both methods (adding MAC] and DMSO) slow the crystal growth and gives rise to larger and more uniform perovskite crystals. Uniform crystals will then prevent the formation of multiple phases, which gives rise to a narrow phase distribution. Thus, by using MAC) and DMSO to slow the crystal growth rate, we have successfully narrowed the phase distribution and changed the carrier flow in the quasi-2D perovskites.

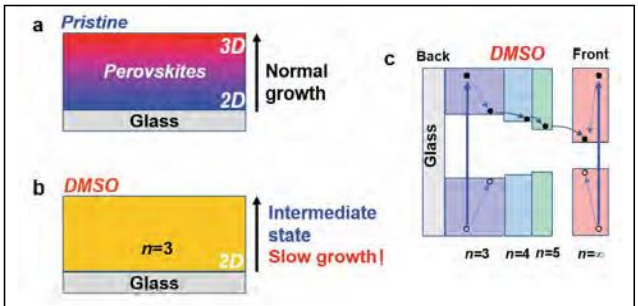

Figure 7. (a-b) Film growth direction and phase distribution of pristine film and film after adding DMSO. (c) Band structure of film after adding DMSO.

3.1.3 Impact of phase purity and vertical distribution on device characteristics

The vertical alignment in the right direction and phase distribution is important for optoelectronic device application. LED requires energy landscape (multiple phases aligned vertically in the right direction) for carrier transport and efficient electron-hole recombination, while solar cell demands highly crystalline film to suppress the carrier recombination and trap. To understand how phase purity and alignment affect the efficiency of quasi-2D perovskite solar cells, we fabricated solar cell devices with pristine film, films treated by antisolvent, MAC!, and DMSO as the active layers in both conventional and inverted device architectures **(Figure 8).**[26] The device with high phase purity (n=3, DMSO) displays highest efficiency, independent of device architecture. Those with multiple phases

show much lower efficiency, suggesting that phase purity can significantly affect the efficiency.

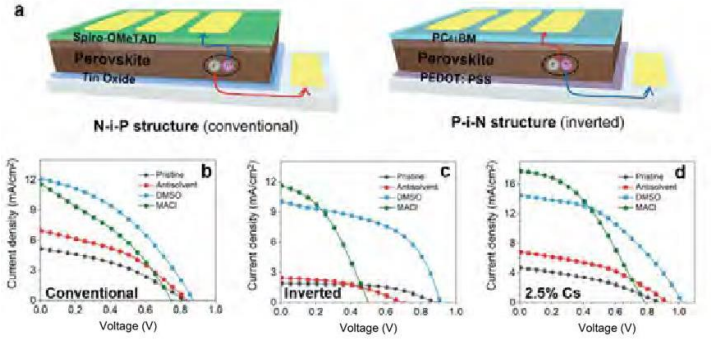

Figure 8. (a) Schematics of conventional and inverted device architectures. *J-V* characteristics of devices with different perovskite films (pristine , antisovlent , DMSO, and MACI) in the (b) conventional structure, (c) inverted structure , and (d) those with Cs in the conventional structure.

In the conventional device architecture, hole is collected by the top anode, while electron is collected by the bottom cathode. Electron flows from lower-n to higher-n phase. Therefore, lower-n phase should segregate at the top in the conventional device architecture. The film with antisolvent (lower-n phase at the top) is aligned in the " right" direction in the conventional device archit ecture, while the device with pristine film (higher-n phase at the top) is aligned in the "wrong" direction. As expected, the conventional device with antisolvent shows higher efficiency than the pristine device **(Figure Sb).** On the other hand, the inverted device architecture collects charges in opposite directions (holes at the bottom anode and electrons at the top cathode). Therefore, the film with antisolvent is aligned in the " wrong" direction in the inverted architecture , while the pristine film is aligned in the "right" direction. As expected, the device treated by antisolvent has lower efficiency than the pristine device. **(Figure Sc)** In order to demonstrate the broad application of tuning the phase purity and vertical distribution and its effect on device characterist ics, we added Cs as the co-cation, which improves the device (DMSO) efficiency to 6.38% **(Figure 8d).** The trend of device efficiency with different phase distributions is maintained. Combined with device cha racterist ics, we have demonstrated the phase purity and vertical alignment are both helpful for optoelectronic device appli cation.

3.2 Self-Assembled Propylammonium Cations at Grain Boundaries and Film Surface to Improve Efficiency and Stability of Perovskite Solar Cells

The major challenge of bringing organic-inorganic hybrid perovskite solar cells towards commercialization is their inherent instability especially with regards to moisture. The introduction of a small amount of hydrophobic cation of large size into a 3D perovskite structure which typically aids in the formation of a quasi-2D perovskite structure is a promising method for maintaining high efficiency while introducing a high stability toward moisture. Despite all the advances achieved in optimizing the device efficiency of quasi-2D perovskites, most efforts so far have been mainly focused on selecting butylammonium (BA) and phenethylammonium (PEA) as large cations to form quasi-2D perovskites. Although a small amount of the large cation is expected to segregate at the film surface to prevent moisture penetration, it has not been straightforward to observe such segregat ion, and how this capping layer affects the surface carrier dynamics remains unclear. In this study, we compare the effects of different large cations such as, ethylammonium (EA), n-propylammonium (PA) and BA cations on the performance and stability of quasi-2D perovskite photovoltaic devices. Our results indicate that the incorporation of a small amount

of PA into the hybrid perovskite active layer aids in the improvement of solar cell performance and stability. To understand such enhancement, we use femtosecond transient absorption and reflection spectroscopy to compare the carrier dynamics in the bulk and at the surface. Our findings suggest that large cations preferentially accumulate at the film surface. We determined that the crystal preferential orien tation, crystallinity , lateral and vertical grain sizes all increase with the incorporation of large cations in particular for PA. This suppresses carrier recombination and prolongs carrier lifetime, ultimately improving device efficiency and stability. Along with enhancements to device stability, the addition of the PA cation significantly improves precursor stabilities. (J. *Mater. Chem. A*, 2019, 7, 23739, *2019 Emerging Investigator Themed Issue)*

Figure 9a summarizes the XRD patterns of a pristine film and those with different cations. After adding EA, PA, and BA, the intensities of peaks are significantly enhanced, suggesting higher degree of crystallinity. The full width at half maximum (FWHM) of the (001) peak decreases after the addition of large cations **(Figure 9b**), while the peak position moves slightly towards low angle, indicating an increased crystallite size and reduced residual stress. We utilized GIWAXS to determine crystal orientation upon the incorporation of large cations within the perovskite bulk **(Figure 9c-e).** Our results demonstrate that the addition of large cations enhances the crystallinity and preferential crystal orientation of the (001) plane normal to the substrate, with PA being the most effective. If the crystallinity and the crystallite size in crease, it should also follow that the grain size would be expected to become larger as well. This was studied with SEM to observe the domain size of the pristine sample and those with the cations EA, PA, and BA. The SEM top-view images show that the average domain size increases with the addition of large-size cations. From the cross-sectional SEM ima ges, multiple domains are formed for the pristine sample along the surface normal while the addition of EA, PA, or BA enables the formation of single domain in the vertical direction.

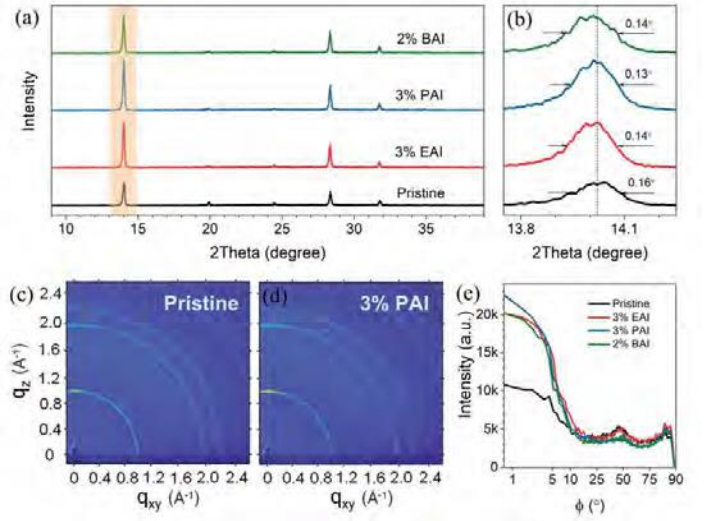

Figure 9 (a) XRD patterns of the films and (b) selected range of plane (001). GIWAXS images of the (c) pristine and (d) 3% PAI films ; (e) intensity as a function of azimuthal angle for q = 1.0 -A ^{1}.

As crystallization and grain size may affect both charge carrier transport and recombination, femtosecond transient absorption (TA) and transient reflection (TR) experiments were performed to study charge carrier dynamics in the bulk and at the surface **(Figure 10).** While the TA spectra of these films are comparable **(Figure 10k),** the kinetics however are slightly different **(Figure 101).** The slightly slower decay through the addition of cations can be attributed to the passivation of the grain boundaries. TA spectroscopy collects the probe

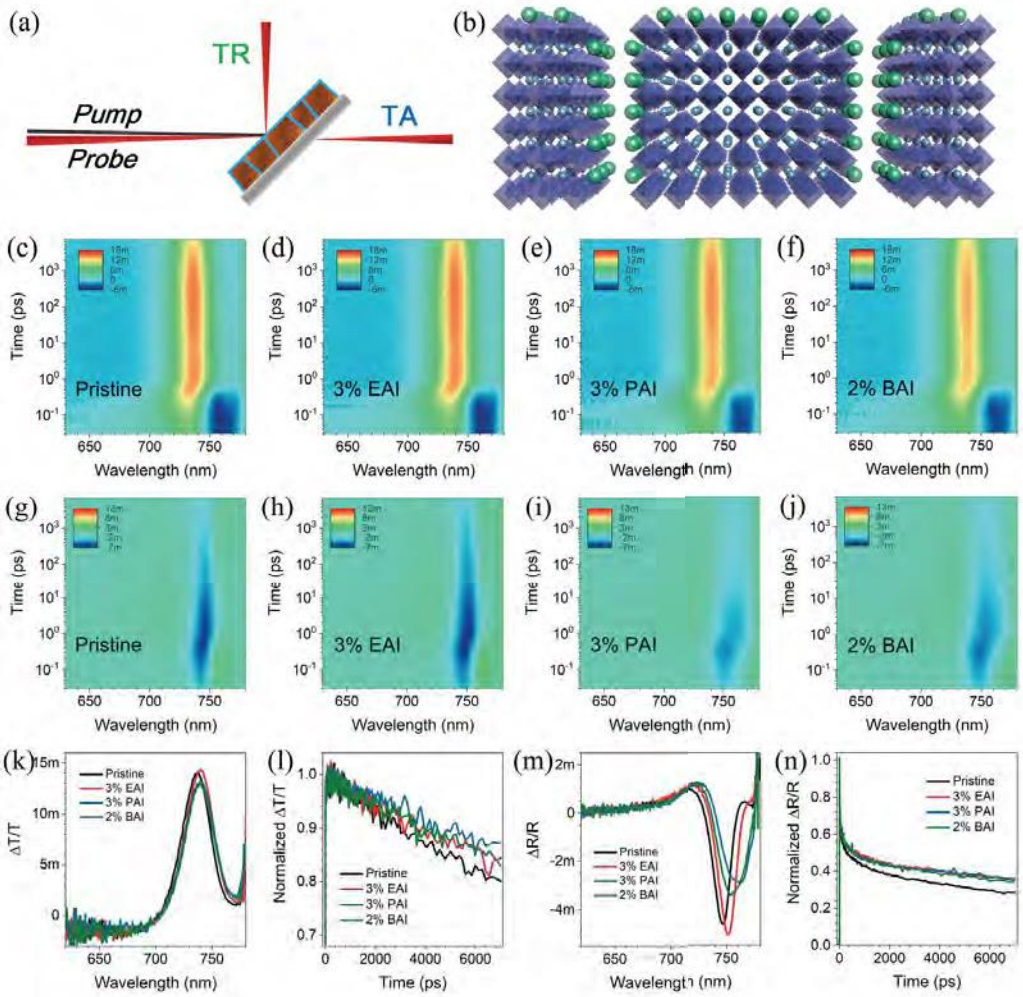

Figure 10 Schematic illustrations of (a) TA and TR spectroscopy; (b) passivation of grain boundaries and film surface by large cations (green balls). (c)-(f) TA spectra and (g)-(j) TR spectra of perovskite films. (k) The spectra at 10 ps and (l) kinetics collected from TA spectra of perovskite films with and without large cations. (m) The spectra at 10 ps and (n) kinetics collected from the TR spectra of above films.

signal transmitted through the entire sample, giving a signal that is integrated over the whole sample. Most importantly, TR spectroscopy collects probe pulses in the reflection geometry causing it to be sensitive to the top 20 nm from the surface (schematic illustration in **Figure lOa).**[28] In contrast to the well-studied recombination in the bulk, surface recombination is still at the early stage. The carrier lifetime of the thin film is limited by surface recombination rather by bulk recombination, highlighting the importance of quantifying the surface carrier lifetime and surface passivatio n. [28] **Figure 10m** and **10n** summarize the spectra and kinetics for perovskite films without and with large cations from TR spectroscopy. We observe that different cations induce ground state bleaching peaks red shifted to different extents with samples containing PA being the most prominent, indicating that the small amount of large cations preferentially accumulates at the surface, forming a heterostructure. Furthermore , the kinetic behavior is different depending on the cation added to the perovskite matrix. The decays in the TR spectra are much faster than those in the TA spectra, indicating that the

density of surface trap states is higher than that of the bulk. The lifetime is prolonged when large cations are incorporated with PA being the most noticeable. These suggest that the large cations that are self-assembling at the surface can prolong the surface carrier lifetime **(Figure 10b**). Given that interfacial trapping is an essential limitation for solar cell devices, we believe that this surface capping with large cations not only prevents moisture from penetrating the perovskite matri x, but also benefits device efficiency.

The device stability without encapsulation in low humidity (10-15% RH) and high humidity (45-50% RH) was tested for devices treated without and with different cations (EA, PA, and BA) **(Figure lla).** As expected, different cations enhance the device stability of mixed ion perovskite solar cells with PA yielding the most stable devices . For example, the efficiency of pristine mixed ion perovskite decreases by 32.1% (from the highest efficiency) while those with PA only decrease by 2.8% after 600 hours.

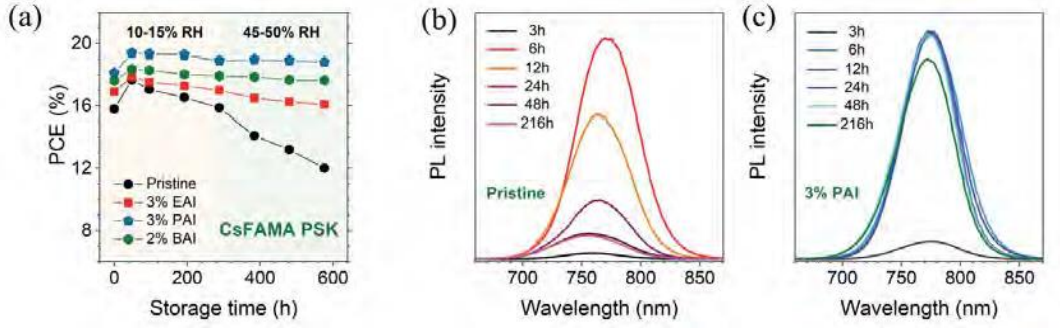

Figure 11 (a) Unencapsulated device stability for mixed ion perovskite cells with and without large cations. Steady-state PL of (b) pristine films and (c) those treated by PAI from precursors with different aging times.

Aside from increasing device stability , in terestingly, we also find that the precursor becomes more stable when large cations are added to the solution. The PL of the pristine film is very sensitive to the aging time of the precursor, while the film treated by PA cations is not sensitive to the aging time of the precursor. This indicates that the PA cations can also stabilize the precursor, leaving a large preparation window for the precursor before its use. We suspect that PA could be absorbed at the surface of perovskite colloid as a ligand, slowing down the phenomenon of Ostwald ripening (small particles aggregate into large particles) to improve the precursor stability. The device performance of PAI contained solar cells (20.1%) changed to 18.7% during the precursor aging process, while the efficiency of pristine device was dramatically decreased after 9 days' aging process (from 18.0% to 13.8%).

3.3 Age-Induced Recrystallization in Perovskite Solar Cells

The highest solar cell efficiency usually appears some time (a couple of days) after the device fabrication, but the underlying mechanism is rarely in the limelight. Here we study device performance under different storage environments. We utilize XRD, time-resolved PL, transient absorption spectrometer, and single-carrier diode measurement to understand the structure and electronic properties of perovskite films for the time scale of weeks. We observe enhanced crystallinity and crystallite size, referred to age-induced recrystallization. Based on the structural changes, the charge trap and recombination are suppressed, while charge transport and collection are enhanced, ultimately improving device efficiency. *(Org. Electron.,* 2019, 68, 143)

We find the device performance increases under nitrogen-filled glovebox environment **(Figure 12a). Figure 12b** display the parameters of perovskite solar cells. The overall performance shows a dramatic increase with the storage time from O day to 2 days, then slowly improves afterwards. The average open-circuit voltage (Voe) shows a sharp increase within the first 4 days, followed by a slight rise. The Voe increases up to 1.19 V after 58 days, which is an impressive value in all the reported results on single-junction solar cells. Overall, the average PCE increases significantly after the storage in nitrogen-filled glovebox environment for four days , from 14.74% to 18.60%. The longer storage in the nitrogen-filled glovebox environment after 58 days can further boost the average efficiency to 19.23% and best efficiency to 20.13%.

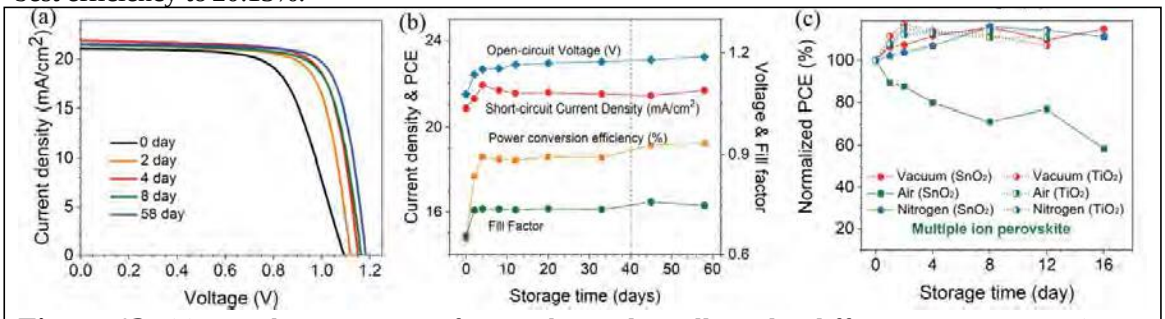

Figure 12. (a) *J-V* characteristics of perovskite solar cells under different storage time (room temperat ure, N_2- filled glovebox environment); (b) Long-term stability of photovoltaic devices. (c) Normalized efficiency of multiple ion photovoltaic devices with TiO2 and SnO2 as electron transport layers as a function of storage time in different environments.

Given perovskite film could be sensitive to the environment of the nitrogen-filled glovebox (solvent, chemical exposure, light exposure etc), we also test the device performance as a function of storage time in three different env ironments, dedicated nitrogen container, vac uum , and dry air. **Figure 12c** displays the normalized efficiency as a function of storage time in three different environments for multiple ion perovskite cells with SnO2 or TiO2 as electron transport layers. We find that device performance generally follows the trend of increasing at the beginning and decreasing afterwards under the storage of dedicated nitrogen container and vacuum . The best efficiency appears between two and eight days. This suggests regardless of the environment, the best device efficiency occurs some time after the device fabrication.

Although the increase of the device performance under inert environment has been observed, the mechanism is much less studied compared with the observation of this unusual phenomenon. Further, this unusual phenomenon is mysterious given that perovskite device is thought to be unstable for long time. To investigate the mechanism , some crystallography and optical characterizations for long-term time scales are utilized. **Figure 13a** shows the XRD patterns of the perovskite films with different storage time in vacuum. The diffraction peak of (001) plane is slightly split as shown in **Figure 13b,** possibly due to the lattice distortion caused by Cs and MA .[29,30] After 4 days' storage, the peak split disappears, indicating the formation of more uniform atomic packing. With the increase of storage time, the peak intensity of plane (001) gradually rises **(Figure 13c),** suggesting that the crystallinity of the polycrystalline perovskite film continually improves. The FWHM of peaks can be used to determine crystallite size according to Scherrer equatio n.[31] As shown in **Figure 13c,** the

decrease in FWHM originates from the increase of perovskite crystallite size and release of residual stress. The shift of peak position towards larger diffraction angle 8 **(Figure 13b and 13c)** suggests the shrinked planes' space. For the specific pla ne, a narrower crystal plane space means more compact atomic packing. The perovskite thin film is deposited by spin coating followed by thermal annealing. Such process happens in an hour, which can create some lattice distortion yielding to residual stress. The residual stress and lattice distortion can be relaxed or recovered by the long-term storage, as shown in **Figure 13d.** The crystallinity

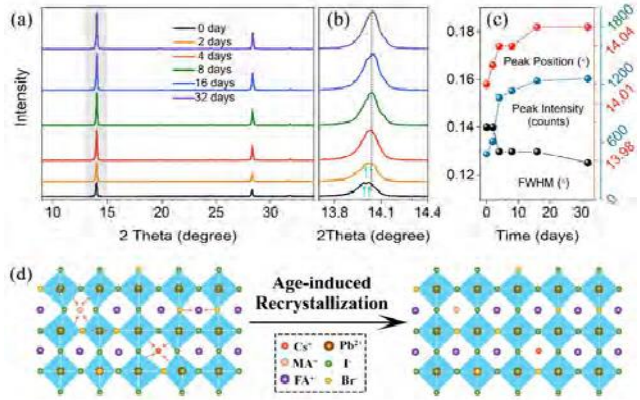

Figure 13. (a) XRD patterns of perovskite films with different storage time in vacuum ; (b) selected range of the major peak; (c) FWHM, peak positions, and intensities of the curves. (d) Schematic illustration of age-induced recrysta llization process.

associated with the peak intensity also increases. We attribute the gradual crystallization (increase of XRD peak intensity and decrease of FWHM) after the film fabrication to the age-induced recrystallization. All these phenomena due to age-induced recrystallization are beneficial for perovskite device application.

Besides XRD, We also utilize time-resolved PL, transient absorption spectrometer, and single-carrier diode measurement to understand the electronic properties of perovskite films for the time scale of weeks. Based on the structural changes during the age-induced recrysta llization, the charge trap and recombination are suppressed, while charge transport and collection are enhanced, ultimately improving device efficiency.

3.4 Manipulating the Growth of $DMAPbI_3$ for Efficient and Stable $CsPbI_3$ Solar Cells

CsPbb exhibits good thermal and photo stability. However, direct mixture of Csl and Pbh cannot produce stable inorganic CsPbb perovskite film. HI is the most effective additive now to keep the black phase of CsPbh. HI accelerates the hydrolysis of solvent DMF to create DMAPbh.[32] This reactant was misunderstood as HPbh , until recent study demonstrates that this mysterious reactant is DMAPbh. Although DMAPbh has been synthesized, the syntheses were focused on powder. Several important questions remain: (1) Is the reactant single crystal or polycrystalline? (2) What is the phase or octahedral connectivity of PbI_6 in DMAPbh? (3) How does this reactant grow? (4) How can we tune the property of DMAPbh? (5) How do the characteristics of DMAPbl3 affect the solar cell efficiency and stability ? To answer these questions, it calls for manipulating the growth of DMAPbh „ characterizing its structure, and probing its roles on CsPbb solar cells. We tuned the synthe s is time and temperature to fabricate DMAPbl3 powder and crystal. Interestin gly, the crystal DMAPbh has different colors, bright orange in the center and yellow at the surface, which can be attributed to different phases. Our results show that the crystal DMAPbh plays a critical role in phase and photo stability of films, as well as device efficiency and stability. (manuscript in preparation)

DMAPbl x is synthesized by mixing Pbb and HI/H20 in DMF at room temperature. HI and

water residue accelerates the hydrolysis of solvent DMF into DMAI.[32] DMAPblx is obtained by washing the solution with abundant ethanol **(Figure 14).** This reactant DMAPblx is important to keep the black phase of CsPbh , but it was misunderstood as HPbh for a while. We carried out proton nuclear magnetic resonance (^{1}H NMR) on DMAPbh dissolved in dimethyl sulfoxide-d 6 (DMSO-d6) to confirm that the reactant is DMAPbh rather than HPbl).

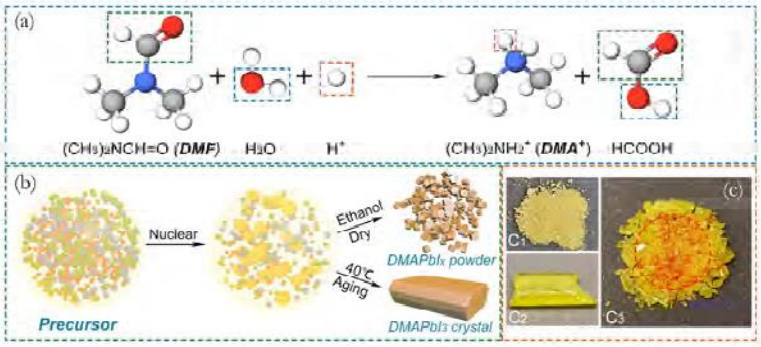

Figure 14. (a) Chemical reaction of DMF, H_20 and HI. (b) Schematic growing process of powder DMAPbl x and crystal DMAPbh. (c) Photographs of powder DMAPblx ($C_{1)}$, crystal DMAPbh ($C_{2)}$ and tiny pieces after breaking the crystal DMAPbh (C3).

The common method , in which the precursor is stored at room temperature for 24h, produces dark yellow powder **(Figure 14c).** We found that the device performance varies from different batches of powder DMAPb,lx This motivates us to reproducible make high quality DMAPbh. Therefore we tune the synthesis time and temperature to manipulate DMAPbh. When the precursor is kept in the oven at 40 °C for 5 days , it grows into yellow crystal with length and width of 5~10 mm **(Figure 14c).** XRD experiments were performed on the large shiny yellow crystals. Surprisin gly, no sharp peaks were observed. This suprising result drives researchers to look into the mystery inside the good-looking crystal. The big yellow crystal was broken into tiny pieces. Interestingly, they have different colors, bright orange in the center and light yellow outside **(Figure 14c).**

To study this interesting phenomen on, steady-state PL and XRD are performed. The single PL peak for powder DMAPblx is observed at 471.6 nm **(Figure 15b).** Two obvious PL peaks exist in the bright orange part of the DMAPbh crystal (C-DMAPbh (0)). The peak at 472.4 nm is similar to the powder DMAPblx, while the other broad peak is at 704.3 nm. For the yellow part of the DMAPbh crystal (C-DMAPbl3 (Y)), the peak at 704.3 nm is very weak. The huge variation in the PL spectra is suspected to be from the difference in bandgap caused by the phase and connectivity of Pbl6 octahedra. When the connectivity of Pbl6 octahedra increases from corner-sharing via edge-sharing to face-shari ng, the dimensionality decreases and the bandgap in creases.[33] According to the large size of DMA+, DMAPbh exhibits 1D structure with face-sharing of Pbl6 octahedra at ambient environment, that is a hexagonal phase. Ther efore, the PL peak at 472.4 nm is from the face-sharing of Pbl6 octahedra at low dimension, while the one at 704.3 nm is attributed to edge- and corner-sharing, corresponding to the trigonal phase **(Figure 15a).** Since the peak at 704.3 nm is broad, the crystal is a mixture of multiple phases, gradually growed from low bandgap (trigonal phase) to high bandgap (hexagonal phase), from corner-sharing and edge-sharing to face-sharing, and from center to outside. Since the bright orange crystal only exists in the center of big crystal, we probe the stability of yellow and orange crystals after 30 min in air. The PL peak at 704.3 nm decreases with time , while the one at 472.4 nm increases accordingly. This suggests the

transformation of unstable corner- or edge-sharing Pbl6 octahedra to more stable face-sharing Pbl6 octahedra. The transformation process could be accelerated by the higher water level at the surface of the crystal. Overall, the PL results suggest that DMAPbh "crystal" is a combination of multiple phases, a gradual growth from unstable structure in the center outwards to stable face-sharing structure.

To further study their properties, the orange part and yellow part crystals were carefully selected for the XRD experiments. The most prominent peaks, corresponding to (100) plane, show different intensities and positions **(Fig 15d-e).** The intensity from the crystal DMAPbh is 1.61 times of that from powder, suggesting higher crystallinity. The peak positions for powder, yellow crystal and orange crystal are 11.59°, 11.60° and 11.66°, respectively. This increase in crystal lattice is consistent with the hypothesis that octahedra connectivity changes from face sharing to corner sharing. The intensity of second peak, corresponding to (201) plane, is significantly different between orange and yellow crystals. Since the peak intensity of the (100) plane increases, it means that the long-range order of the crystal has not been significantly weakened. Therefore, the most likely cause of the decrease in peak intensity of the (201) plane is the small angle distortion between the atomic layers. We suspect the actual difference could be larger than our experimental observation, since orange crystal is extremely unstable in ambient environment.

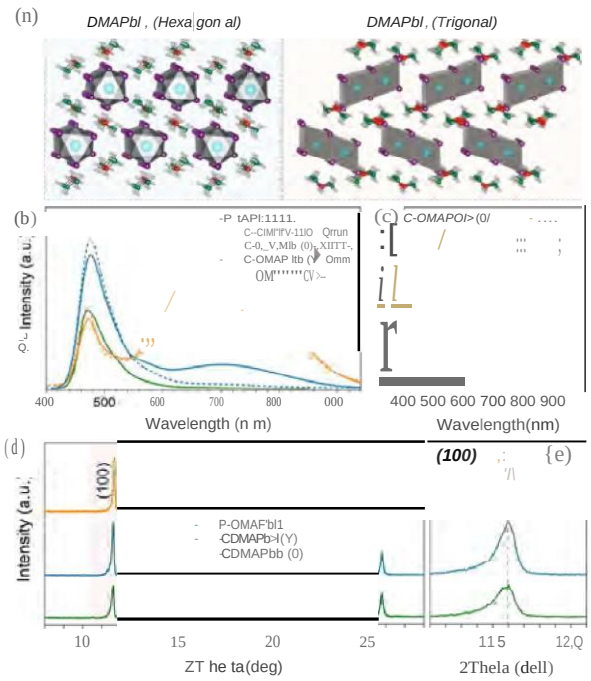

Figure 15. Characterization of DMAPbh. (a) Crystal structure of hexagonal $DMAPbI_3$ and trigonal DMAPbh. (b) Steady-state PL spectra of the powder DMAPblx, orange part and yellow part of DMAPbh crystal, and the spectra of the crystal after 30 min in air. (c) Fitted lines of PL. XRD patterns in the (d) whole range and (e) selected range of plane (100).

CsPbh is fabricated from the precursor, mixture of DMAPbh and Csl. PD-CsPbh and CD-CsPbh represent CsPbh films fabricated from powder DMAPbl x and crystal DMAPbh , respectively. There was a debate whether DMA stays in the final solid thin film. Recently , it has been confirmed that thermal annealing ~180°C converts DMAPbh to -CsPbh .[34] We thermally anneal our samples at 215°C, to transfer to CsPbb. To understand the effects of DMAPbh on the film quality of $CsPbI_3$, XRD was utilized to probe the crystal structure of PD-CsPbh and CD-CsPbb. Our results suggest that black phase of CD-CsPbh made from crystal DMAPbh has better phase stability. Femtosecond transient absorption spectroscopy was utilized to probe the carrier lifetime. The carrier lifetime for CD-CsPbb doubles compared to that for PD-CsPbb. Moreover, the lifetime is reproducible for CD-CsPbb after

femtosecond laser illum ination , while it decreases for PD-CsPbb , suggesting that CsPbb fabricated from crystal DMAPbI 3 is more photo stable.

To probe the effects of DMAPbb ondevice characteristics, we fabricate solar cells with an architecture of FTO/TiO2/ CsPbh /Spiro-OMeTAD /Ag. **(Figure 16)** The devices made with PD-CsPbI 3 display an average efficiency of 15.03 ± 0.92 %. With CD-CsPbh , device characteristics are improved to efficiency of 17.41 ± 0.60 %. The champion device efficiency , 18.07% , is among the top few records of CsPbh, More impo rtant ly, the devices comprising CD-CsPbh show significantly better stability. The efficiency of device comprising PD-CsPbh drops from 16.58% to 0.23% after 50 days' storage under the humidity of 20-30% RH without encapsu latio n, while that comprising CD-CsPbI3 decreases from 18.07% to 14.13%. This is consistent with our characterization of CD-CsPbh that has higher crystallinity , fewer grain boundaries, and longer carrier lifetime.

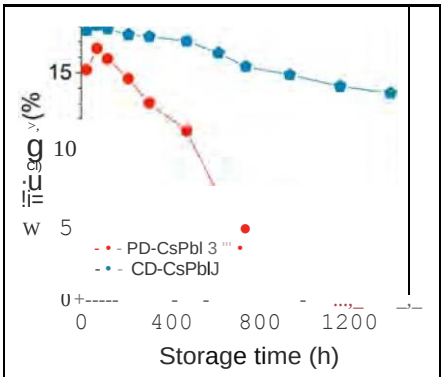

Figure 16. Long-term stability of devices comprising PD-CsPbI3 and CD-CsPbh.

3.5 Effect of Composition on the Spin Relaxation

Besides energy conversion and light emission , spintronics is a promising application for perovskite.[35, 42] The application of spintronics requires semiconductors that allow efficient spin generation and transport at room tempe rature.[43-45] Lead halide perovskites exhibit strong spin orbital coupling (SOC),[46,47] making it easier to manipulate spin and spin-polarized current at room temperature. However, strong SOC typically reduces spin life time ,[46, 48] which may limit their spin transportation. Both experimental and theoretical work have reported a large Rashba effect in perovskite with the coexistence of SOC and inversion symmetry breaking,[49,, 54] which is very important for electric spin manipulation. The easy tunability of bandgap and SOC of perovskite makes it possible to design an ideal device for spintronic applic ations .

In a spintronic device , information is recorded in the spin state of electrons while the spin state relaxes by scattering with carriers and phonons during the transportation. [55,, 57] Understanding the mechanism behind spin relaxation is therefore of great importance for their real applications. For III-V group inorganic sem ico nductors , three spin relaxation mechanisms including Elliot-Yafet (E-Y),[58, 59] D' yakonov-Perel (D-P)[60] and Bir-Aronov-Pikus (BAP)[61] were proposed and experimentally proved. In E-Y mechanism , spin relaxation is induced by spin-orbit interaction and charge carrier can flip their spin upon scattering. [56] D-P mechanism often occurs in the system without center of inverse symmetry , in which both Dresselhaus (bulk inversion asymmetry) and Rashba (structure inversion asymmetry) effects might induce spin precession randomized by sca ttering.[37, 46] BAP is responsible for those heavy p-doped semiconductors , where electrons and holes experience spin flip scattering via Coulomb exchange coupling. In contrast to those of III-V semiconduc tors, study on the spin relaxatio n of perovskite is still at the early stage. Less is known about the spin dynamics of different perovskites and the detailed mechanism behind is still unclear. Therefore , a comprehensive investigation on the spin relaxation of perovskite with different compositions at different temperatures is needed to get a better understanding

on the spin relaxation.

We investigate the spin relaxation dynamics of several perovskite thin films with different compositions at different temperatures by circular polarized transient absorption spectroscopy. It is found that at room temperature, the net spin relaxation time increases from 1.2 ps to 4.3 ps as the molar mass of anions and cations decreases, indicating that SOC largely determines the spin lifetime at room temperature. When the temperature decreases from room temperature to 77 K, it is found that MAPbb and CsPbh show more rapid increase in spin lifetime compared to $MAPbBr_3$ and $CsPbBr_3$. Detailed analysis on the spin relaxation shows that E-Y mechanism is more likely to be responsible for the spin relaxation for MAPbh and $CsPbI_3$ while D-P is more likely to explain the spin relaxation for $MAPbBr_3$ and $CsPbBr_3$. Our work for the first time illustrates the effect of composition on the spin relaxation and mechanism of perovskites and will stimulate future research on spin dynamics and spintronic devices. *(J Phys. Chem. Lett.,* 2020, 11, 1502)

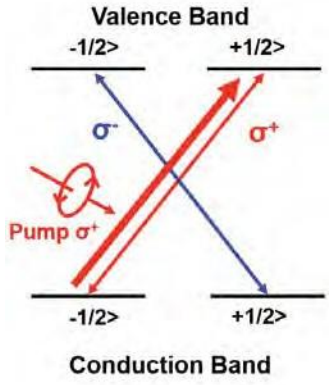

Figure 17. Selection rule in circular polarized pump-probe experiment.

As shown in **Figure 17,** we used a circular polarized pump-probe experiment method:[46] a left circular polarized (e+r) pump pulse was used to excite the sample and both left (er+) and right (er-) circular polarized pulses were used to probe the sample. e+r pump pulse will induce the transition from |112, -1/2> to the |112, +1/2> spin state (increasing angular momentum by *+n)* and each probe polarization will trace the different m_1 states (projection of total angular momentum quantum number onto z-axis). The net spin relaxation is calculated by the difference between the c+r and -cr probe signals , which is the difference between the population of mi=+1/2 and mi=-1/2 of both electron and hole.

Figure 18 A-D show the spin relaxation of four perovskite films at room temperature measured by circular polarized transient absorption (TA). When pump and probe have the same polarization (co-circular), the probe pulse measures the state filling response so that it probes the majority spin population. When pump and probe have the opposite polarization (counter-circular), the probe pulse measures the minority of the spin population and finally these two population will be the same after the spin relaxation occurs. As shown in **Figure 18A,** the co-circular TA signal of MAPbb experiences a decay in the first 10 ps while the counter-circular TA signal sees a rise at the same time. The net spin is calculated as the difference between co- and counter-circular TA signals and fitted using a single exponential decay to give a lifetime of 2.2 ps. The net spin relaxation of $MAPbBr_3$ **(Figure 18B)** gave a lifetime of 4.3 ps, almost twice of that of $MAPbI_3$. As shown in **Figure 18CD,** after MA is replaced by inorganic Cs, the room temperature net spin relaxation lifetime r_5 is decreased to 1.3 ps for CsPbh and 3.7 ps for CsPbBr3.

The spin relaxation lifetime is strongly related to the degree of phonon scattering and Rashba-Dresselhaus splitting. Typically, strong phonon scattering decreases the spin lifetime because it gives rise to faster spin randomization and flip.[62] Rashba splitting, induced by SOC and symmetry breaking , was reported to increase the spin lifetime.[63] It is interesting to see the spin lifetimes of four perovskite thin films follow the order:

MAPbBr3> CsPbBr3> MAPbb >CsPbh and the spin lifetime at room temperature decreases as the molar mass of cations and/or anions increases while anion has a stronger effect. To further understand the effect of anion molar mass, we also prepared MAPbIBr2 and MAPbbBr and compared their spin relaxation dynamics with MAPbh and MAPbBr3 and the room temperature net spin lifetime versus the molar mass of all perovskite films was plotted **in Figure 18E.** It is found that the spin lifetime of MAPbIBr2 and MAPbbBr (3.3 ps and 2.3 ps, respectively) lie between that of MAPbBr3 and MAPbI3 (4.3 ps and 2.2 ps, respectively). Such an observation is consistent with the fact that heavy atom should lead to strong SOC and thus shorter spin lifetime. [43, 46] Based on our observation and discuss ion, the molar mass (heavy atom effect) should explain the difference in the room temperature spin lifetime of perovskite with different compositions.

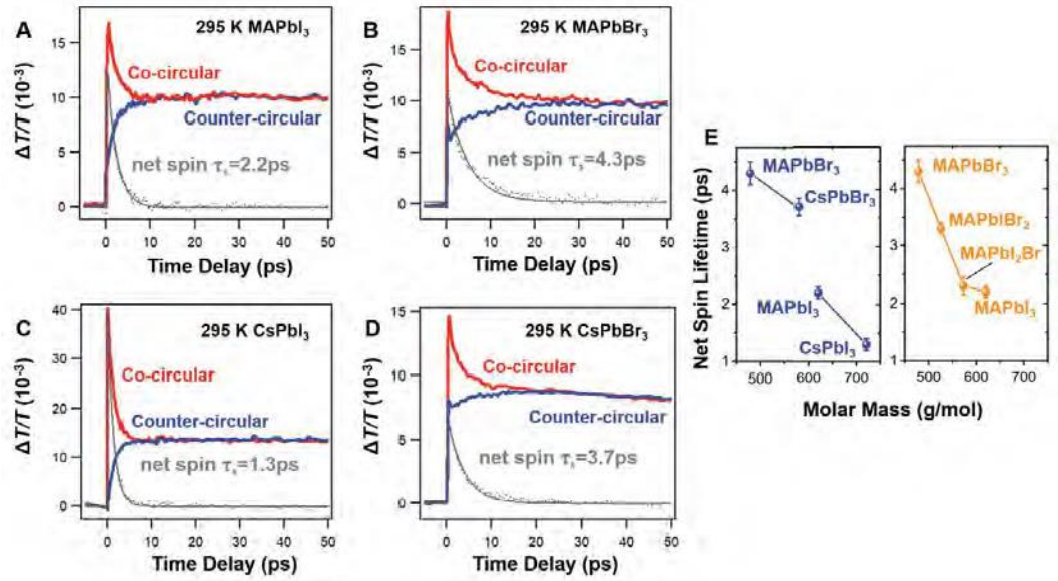

Figure 18. The co- and counter-circular polarized pump-probe kinetics with their difference of (A) MAPbI3, (B) MAPbBr3, (C) CsPbh and (D) CsPbBr3 at room temperature. (E) Net spin lifetimes versus molar mass of perovskite films with different cations and anions at room temperature.

Three mechanisms including E-Y, D-P and BAP were reported to be responsible for the spin relaxation in inorganic semiconductors. BAP mechanism is applicable to heavy p-doping semiconductors so that it is not considered for perovskite, [46] while both E-Y and D-P can be used to explain the spin relaxation in perovskite. In E-Y mechanism for III-V group semiconductors , the spin lifetime can be written as: [55]

$$\frac{1}{\tau_s} = A\left(k_B T\right)^2 \frac{\Delta^2/\left(1-\Delta/2\right)}{E_g} \frac{1}{\tau_p} \qquad (1)$$

where τ_p is the momentum relaxation time, E_g is the bandgap, $\Delta = \Delta_{so}/(E_g+\Delta_{so})$ with spin orbit splitting of the valence band Δ_{so} and A is a dimensionless constant. In D-P mechanism for III-V group semiconductors where Dresselhaus effect dominates, the spin lifetime can be written as : [60]

$$\frac{1}{\tau_s^{DP}} = Q\alpha^2 \frac{\left(k_B T\right)^3}{\hbar^2 E_g} \tau_p \qquad (2)$$

where Q is a dimensionless constant and a is given by:

$$a = \frac{m_e}{3 \cdot 17 m_o} \quad (3)$$

in which *me* and *mo* are the effective mass of the conduction electrons and the electron rest mass, respectively. For both Rashba and Dresselhaus effects, one can found that phonon scattering plays different roles in E-Y and D-P mechanisms , where rs is proportional and inversely proportional to *rp,* the momentum relaxation lifetime , respectively. As both r_s^{EY} and τ_s^{DP} are sensitive to tempe rature, it should be helpful to understand the mechanism by measuring temperature dependent spin relaxation of those perovskite films.

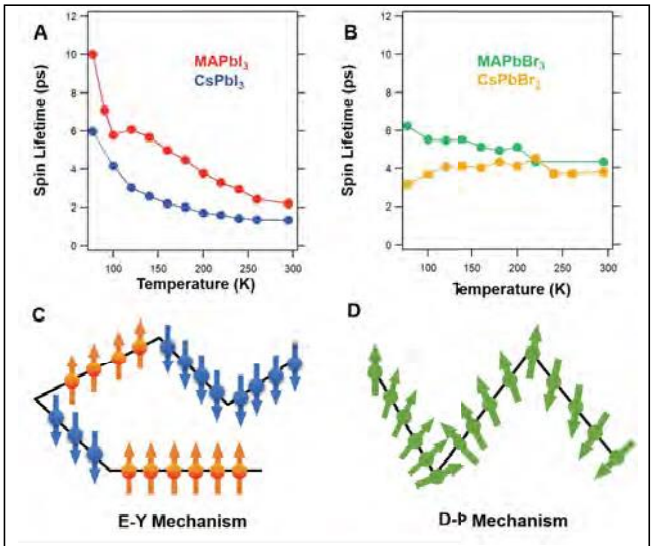

Figure 19. (A) Net spin lifetime versus temperature of MAPbh and CsPbh thin films; (B) Net spin lifetime versus temperature of MAPbBr3 and CsPbBr3 thin fi lms; (C) Schematic diagram of E-Y mechan is m; (D) Schematic diagram of D-P mechanism.

We performed circular polarized TA measurements between 295 K and 77 K for all four perovskite films. The net spin lifetimes versus temperature are plotted in **Figure 19 AB.** For both MAPbh and CsPbh , one can observe significant increase in spin lifetime rs as the temperature is reduced between 295 Kand 120 K (rs increases from 2.2 to 6.1 ps for MAPbh and from 1.3 to 3 ps for CsPbh). In MAPbI3, r s decreases from 120 K to 100 K and then increases rapidly at lower temperatures (rs is 10 ps and 6 ps for MAPbI3 and CsPbh at 77 **K,** respectively). In CsPbh , there is no abrupt change in rs and it also increases more significantly at lower temperatures *(T*< 150 K). The abrupt change at 120 K for MAPbI3 should be related to the phase transition from tetragonal to orthorhombic phase, which is absent for CsPblJ_ On the other hand, in MAPbBr3 and CsPbBr3, there are only subtle changes in the spin lifetimes. From 295 K to 77 K, rs increases from 4.3 to 6.2 ps for MAPbBr3 and decreases from 3.8 to 3.2 ps for CsPbBr3.

The different temperature dependence in rs for perovskite with iodide and bromide should be related to different mechanisms of spin relaxation. To study the effect of phonon scattering on spin lifetime , we use E-Y and D-P mechanisms to understand our observations. As shown in equation (1) and (2), $\tau_s^{EY} \propto \tau_p / T^2$ and $\tau_s^{DP} \propto \tau_p / T^3$ so that spin lifetime should increase as temperature is reduced at first glance. However, since $\tau_s^{EY} \propto \tau_p$ and $\tau_s^{DP} \propto \tau_p$, momentum relaxation plays an opposite role in E-Y and D-P mechanisms , respectively. This is attributed to the fact that spin flips during momentum scattering for E-Y, while spin relaxes between momentum scattering for D-P mechanism. When the temperature is reduced, phonon scattering becomes weak and thus the momentum relaxation slows down (rp will increase). Overall, *rs* should increase when temperature is reduced for EY, but *Ts* does not have to follow this monotonous trend and can become complicated for D-P mechanism. As

temperature is reduced, we observed a significant increase in τ_s of I-based perovskite and a subtle change in τ_s of Br-based perovskite **(Figure 19AB).** As a result, it is more likely that D-P dominates the spin relaxation in Br-based perovskite ($MAPbBr_3$ and $CsPbBr_3$) while E-Y dominates the spin relaxation in I-based perovskite (MAPbb and CsPbb) **(Figure 19 CD).**

3.6 Charge Transfer and Diffusion at the Interface

A typical perovskite solar cell is made of multilayers, with perovskite sandwiched by electron transporting layer (ETL) and hole transporting layer (HTL).[64-66] Efficient charge transfer (CT) between perovskite and electron/hole extracting layer is a key step in a working device.[67,68] Time resolved spectroscopy has been used to study the CT between perovskite and different electron or hole acceptors and the reported CT time in literatures varies from sub-picoseconds to nan oseconds.[67,76] Most of previous studies used transient absorption spectroscopy (TA) to study the CT dynamics between perovskite and acceptor.[70,71,77-79] In TA measurements , the pump and probe pulses travel through the entire film and the obtained signal reflects the bulk properties of the sample.[80,81] Transient reflection (TR) spectroscopy, on the other hand, probes the difference of reflected probe light *(!).R/R)* with and without pump pulse. Unlike TA, TR detects the change in the photoinduced reflection of the sample surface so that it will reflect surface recombination dynam ics.[28,82] Therefore, TR spectroscopy is more suitable for detecting the interfacial charge transfer and energy transfer in thin films. Moreover, establishing a suitable model to resolve the surface recombination rate and diffusion coefficient is of importance to under stand how interfacial CT is determined by surface morphology.

We combined TA and TR spectroscopies to study the interfacial CT and diffusion dynamics between $MAPbI_3$ and [6,6]-phenyl-C61-but yric acid methyl ester (PCBM). Steady state and time resolved photoluminescence indicates that there should be efficient CT from MAPbb to PCBM. Although there is no additional ultrafast CT observed in TA , a sub- picosecond charge transfer coupled with carrier diffusion was observed in TR kinetics after coating a MAPbb film (1 M concentration) with PCBM. Interestin gly, the interfacial CT process significantly slows down in a thinner film (0.25 M concentration), which was explained by more significant surface recombination and carrier diffusi on. A diffusion-based model was further established to fit the TR dynamics , and surface recombination rate and diffusion coefficient of different films was compared. The observation of diffusion coupled CT from MAPbb film to PCBM will stimul ate future work on the CT study on perovskites. *(J. Phys. Chem.* C, 2019, 123, 22095)

The TA results were shown in **Figure 20 A-D.** In the TA spectra *(iJT/T),* the positive signal represents ground state bleaching (GSB) and the negative signal stands for excited state absorption (ESA). In the film coated with PCBM, similar spectra features can be observed in the initial 1 ps **(Figure 20B).** On the other hand , the TA decay after 100 ps accelerates significantly in film coated with PCBM **(Figure 20D),** which indicates efficient charge transfer. In contrast to TA, TR probes the change in the real part of the refractive index, which is relatively more sensitive to the film surface.[28] The TR measurements were performed under the same carrier density, with incident angle of 45 degree. It is found that *iJR /R* shows opposite spectral features to that of *iJT /T,* with GSB showing negative signal **(Figure 20 E, F).** In general, the TR signal decays faster than TA, which could be explained by both carrier diffusion into the film and stronger surface recombination. A closer look at the decay of *iJRIR* at the GSB maxima indicates that in the film with PCBM, a stronger

sub-picosecond decay can be clearly observed **(Figure 20H).** By performing multi-exponential decay convoluted by instrument response , the sub-picosecond decay in MAPbh:PCBM film is determined to be 450 fs. Detailed global analysis was carried out.

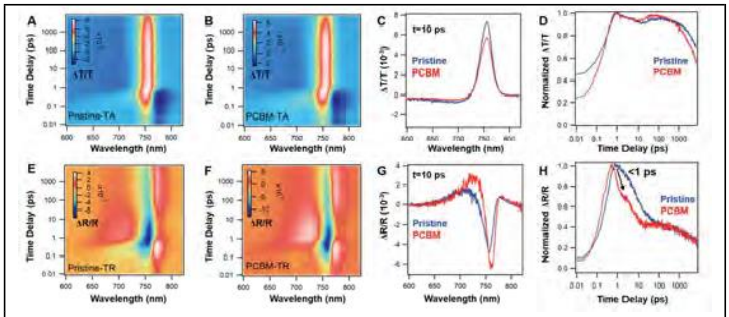

Figure 20. (A-B) TA data map of 1 M films; (C) TA spectra of two films probed at 10 ps; (D) Normalized TA decay traces of two films probed at GSB maxima ; (E-F) TR data map of two films; (G) TR spectra of two films probed at 10 ps; (H) Normalized TR decay traces of two films probed at GSB maxima.

As shown in **Figure 21A,** the TA data of 0.25 M pristine film shows much shorter lifetime compared to that of 1 M **(Figure 20A)** and it decays to less than 10% of the initial intensity within 8 ns. It is found that adding PCBM further accelerated the decay while the spectral features remained the same **(Figure 21B-D).** Compared to the TA kinetics of pristine film, there is an additional fast decay between 1 ps and 100 ps in the MAPbh/PCBM film and the decay time constant is around 11 ps, much slower than that in 1 M film. Such an additional decay should be ascribed to the CT

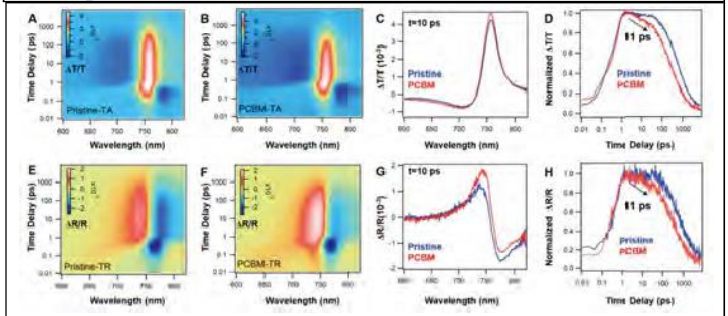

Figure 21. (A-B) TA data map of 0.25 M fi lms; (C) TA spectra of two films probed at 10 ps; (D) Normalized TA decay traces of two films ; (E-F) TR data map of 0.25 M films; (G) TR spectra of two films probed at 10 ps; (H) Normalized TR decay traces of two films.

from perovskite to PCBM. Detailed global analysis was described in the paper *(J Phys. Chem.* C, 2019, 123, **220951** We didn' t observe any additional ultrafast process less than 1 ps in PCBM coated 0.25 M film, which indicated no ultrafast interfacial CT was observed. Instead, there is an additional 11 ps decay in PCBM coated perovskite films, which is similar to that observed in TA and should be assigned to interfacial CT. If one compares the kinetic decays of TA at 760 nm and TR at 740 nm, it is found that the normalized TA and TR kinetics are almost identical for both pristine film and PCBM coated film. These observations further indicate that TA signal has strong contribution from TR and thus surface recombination dominated the TA signal. Those pinholes observed in 0.25 M by SEM should explain the stronger surface recombination.

Carrier dynamics and distribution of perovskite film is determined by carrier diffusion, surface and bulk recomb inat io n. [28] To quantitatively extract the diffusion coefficient and surface recombination rate in 1 M and 0.25 M fi lms , we further performed fitting based on the following equations: [79]

$$\frac{dN}{dt} = D\frac{d^2N}{dx^2} - \frac{N}{\tau} \quad (4)$$

$$\frac{dN(x,t)I}{dx}_{X=O} = \frac{s\ f\ ron}{D} N(O,t) \quad (5)$$

$$\frac{dN(x,t)I}{dx}_{X=l} = -\frac{s\ back}{D} N(L,t) \quad (6)$$

where $N(x,t)$ describes the carrier density as a function of the film depth *'x'* and of the time *'t'*, D is the diffusion coefficien t, τ is the bulk carrier lifetime, S_{Jront} and S_{back} are front and back surface recombination rates, respectively. Equation 5) and Equation 6) are the Neumann boundary conditions for the carrier density with L being the thickness of the film (L = 280 nm for 1 M film and L = 60 nm for 0.25 M). As the equation and boundary conditions are writ ten, there is no explicit solution to describe the carrier density. To fit our model to the data, we used the finite backward difference method on Equation 4), and the finite central difference method on Equation 5) and Equation 6). The fitting of kinetic traces of two films based on the proposed model leads to two distinct sets of constants for the 1 M and 0.25 M films as shown in **Table 1.** Since the TR dynamics is strongly dependent on probe wavelength, we choose to fit the dynamics with most significant diffusion decay component based on the global fitting results.

Table 1. List of best fitting parameters for 1 Mand 0.25 M films.

Concentration	**D (cm^2/s)**	**Srront(cm/s)**	Shack **(cm/s)**	τ **(nanosecond)**
lM	0.05	420	420	200
0.25M	0.005	850	460	20

In IM film, the front and back excitation gives similar decay dynamics so that S_{front} and S_{back} are the same. In 0.25 M film, front excitation shows faster decay than that of back excitation so that S_{front} is higher than S_{back}. As the decay in the carrier density of the 0.25 M film is more rapid than in the 1 M film. That is attributed to the 0.25 M films having more surface defects than the 1 M films; this is also reflected in their values for the surface recombination rate where S for the 0.25 M films is almost two times larger than the S for the 1 M film. The bulk carrier lifetime of the film is also ten times longer in the 1 M film than in the 0.25 M film, allowing for a slower decay. Those pinholes observed in the 0.25 M film by SEM should account for more trap state and strong surface recombination, which would compete with interfacial CT and reduce the CT efficiency.

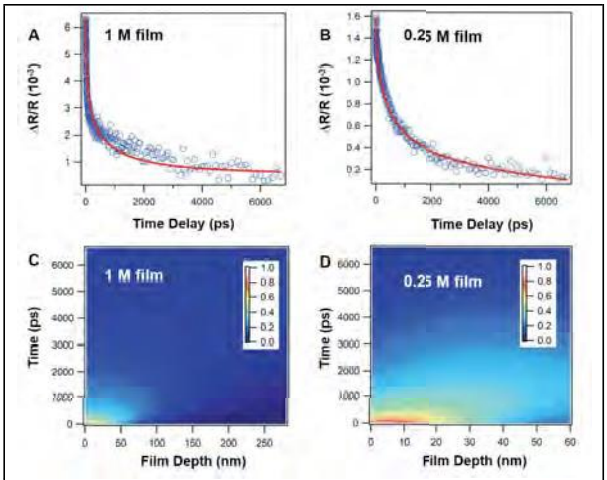

Figure 22. TR decay trace and fit for (A) 1 M film and (B) 0.25 M film. Carrier density as a function of time and film depth in the (C) 1 M film and (D) 0.25 M film.

Based on the diffusion coefficient D and surface recombination rate S in **Table 1,** we further plot normalized $N(x,t)$, the carrier density as a function of time and position, in **Figure 22 C and D.** In the 1 M film, it is found that the relaxation dynamics is significantly different for

front (x=0 nm) and back (x=280 nm) surface **(Figure 22C).** The front surface saw a rapid decay in the first 0.2 ns and a very slow decay in the following 6 ns, while the carrier density at x= l 00 nm saw a rise in the initial 0.2 ns followed by a slow decay. The initial rapid decay in the front surface and the initial rise in the dynamics at x=l00 nm, respect ively , sho uld be explained by the diffusion of carriers from higher to lower carrier concentration region. In the 0.25 M film, on the other hand, the front surface saw a rapid decay in the first 1 ns followed by a relatively slower decay to almost zero between 1 and 6 ns while the back surface saw a rise in the first 1 ns followed by a slow decay.

3.7 Generation of Coherent Optical Phonon in Perovskite

Long-lived hot carrier in orgamc-morganic hybrid perovskite materials is possibly assisted by the large polaron and hot phonon bottleneck. Phonon plays a significant role in the properties of hybrid perovskite. Coherent phonon refers to the in-phase vibration of crystal lattice. Here, temperature-dependent , fluence-dependent , and polarization-dependent transient absorption spectroscopy is utilized to study the coherent phonon in MAPbh. The coherent optical phonon **(Figure 23)** is observed due to the existence of Pb-I-Pb angular distortion at 24-33 cm^{-1} in both tetragonal and orthorhombic phases. The oscillation from the excited state absorption is also observed, suggesting the couple between coherent phonon and photo-excited state. The oscillation of coherent phonon attenuates with increasing environmental temperature. The dependence of coherent phonon on the polarization of the pulse and the quantitative analysis indicates the generation mechanism is impulsive stimulated Raman scattering and transient depletion field screening. (Details in *J Phys. Chem.* C, 2018, 122, 17035)

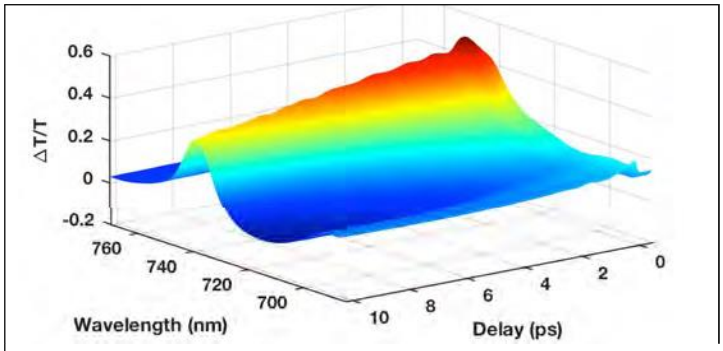

Figure 23. Coherent phonon in hybrid perovskite.

4. Future

We have been using femtosecond visible transient absorption spectroscopy to study carrier dynamics in metal halide perovskites. Our platform provides unique opportunities to stud y materials beyond metal halide perovskite. For example, the materials we have studied and will continue to study include organic ligand protected metal nano cluster , graphene , organic semico nductor , 2D mater ial, quantum dot, etc. The optoelectronic application can go beyond solar cells, such as spintronics , las ing, light-emiss io n, etc. Structure-photophysics-function relationship will be used as a unifying strategy to search new optoelectronic materials and novel device application.

To further probe the vibrational dynam ics , and combine the temporal and spatial reso l utio ns, we recently submitted a DURIP proposal, which is for the acquisition of advanced time reso lved spectroscopy that includes mid-IR transient absorptio n spectroscopy and transient absorption microscope. The control number of the proposal titled "Time Resolved Spectroscopy for Vibrational Dynamics and Imaging of Materials" is 20RT0492. (Tracking Number: GRANT13 l 03615). Ultrafast pump-probe electronic spectroscopy (UV-visible) probes the electronic transitions between delocalized orbitals. It lacks the ability of probing

site-specific information of structural change, and strong overlaps of electronic transitions may complicate the interpretation of experimental results. Femtosecond UV-vis pump mid-IR probe spectroscopy is a powerful tool to investigate ultrafast structural dynamics. Moreover, the dephasing time of vibration is longer than that of electronic transition, resulting in narrower IR absorption and easier data analysis. With femtosecond UVNis pump Mid-IR probe spectroscopy, it is possible to observe ultrafast photoinduced structural and conformational dynamics initiated by electronic excitation. Combining with ultrafast pump-probe electronic spectroscopy in our lab, we plan to probe the structural dynamics of perovskites, organic semiconductors, organic ligand protected metal nanoclusters, etc.

Although ultrafast time resolved spectroscopy offers the time resolution to probe carrier dynamics, it is performed on large ensembles of molecules in solutions or films, which provides no spatial information. Transient absorption microscope (TAM) combines spatial resolution and temporal resolution. The function of optoelectronic materials and systems depends on photo-induced process in a short time and molecule spatial distribution. With TAM, we can image the energy and charge transport over long distance in different organic and hybrid materials.

List of Publications and Significant Collaborations that resulted from AFOSR supported project:

a) papers published in peer-reviewed journals

10 Journal papers on this grant (six as corresponding author and four as co-author)

1. M. Zhou, J. Sarmiento, C. Fei, X. Zhang, **H. Wang*.** " Effect of Composition on the Spin Relaxation of Lead Halide Perovskites" *J. Phys. Chem. Lett.*, **2020,** 11 , 1502.
2. C. Fei, M. Zhou, J. Ogle, D.-M. Smilgies , L. Whittaker-B rooks, **H. Wang*.** " Self-Assemb le d Propylammonium Cations at Grain Boundaries and Film Surface to Improve Efficiency and Stability of Perovskite Solar Cells" *J. Mater. Chem. A,* **2019,** 7, 23739. **(2019 Emerging Investigator Themed Issue)**
3. M. Zhou, C. Fei, J. S. Sarmiento, **H. Wang*.** " Man i pulati ng Phase Distribution and Carrier Transfers in Hybrid Quasi-Two-Dimensional Perovskite Films" *Solar RRL,* **2019,** 3, 1800359. (This article also appears in hot topic: solar cells)
4. C. Fei, **H. Wang*.** "Age-Induced Recrystallization in Perovskite Solar Cells" *Org. Electron.,* **2019,** 68 , 143.
5. M. Zhou, J. Sarmiento , C. Fei , **H. Wang*.** " Charge Transfer and Diffusion at the Perovskite/PCBM Interface Probed by Transient Absorption and Reflect io n" *J. Phys. Chem.* C, **2019,** 123, 22095.
6. C. Fei, J. Sarmie nto, **H. Wang*.** "Generation of Coherent Optical Phonon in Methylammonium Lead Iodide Thin Films " *J. Phys . Chem.* C, **2018,** *122,* 17035.
7. M. Tit ze, C. Fei, M. Muno z, X. Wang , **H. Wang,** H. Li*. " Ultrafast Carrier Dynamics of Dual Emissions from Orthorhombic Phase in Methylammonium Lead Iodide Perovskites Revealed by Two-Dimensional Coherent Spectroscopy" *J. Phys. Chem. Lett.*, **2019,** 10, 4625. (Journal Cover)
8. X. Shan, S. Zhang, M. Zhou, T. Geske, M. Davis, A. Hao, Z. Liang, **H. Wang,** Z. Yu*. "Porous Halide Perovskite-Polymer Nanocomposites for Explosive Detection with A High Sensitivity" *Adv. Mater. Inter.,* **2019,** 6, 1801686.
9. J. Li, J. Lu, A. Chew, S. Han, J. Li , Y. Wu, **H. Wang,** S. Ghimire, Z. Chang*. Attosecond Science based on High Harmonic Generation from Gases and Solids. *Nat. Commun.,* **2020,** 11, 2748.
10. Y. Li, M. Cowan, M. Zho u, M. Taylor, **H. Wang,** Y. Song, G. Mpourmpakis, R. Jin*. "Heterometal-Doped M23 (M=Au/Ag/Cd) Nanoclusters with Giant Dipole Moments" *ACS nano,* **2020,** 14, 6599.

b) papers published in non-peer-reviewed journals or in conference proceedings

None

c) conference presentations

1. Steven Institute of Technolog y, Chemical Engineering & Materials Science, NJ, February 2020.
2. OSA Advanced Photonics Congress, on li ne, July 2020.
3. SPIE Optics+ Photonics , on line , August 2020.
4. Southeastern Section of the American Physical Socie ty, Wrightsville Beach, NC, November 2019.
5. 2019 Florida American Vacuum Society Sympos ium, Orl ando , March 2019.
6. University of Central Flo rida, Physics Department, O rlando, January 2019.
7. 21st Annual Southeast Ultrafast Conference (SEUFC' 18), Atlanta, August, 2018.

8. Florida International University, October, 2017.
9. Stanford Linear Accelerator Center (SLAC) THz UED workshop, March, 2017.

d) manuscripts submitted but not yet published

1 submitted and 1 in preparation

1. Y. Song, Y. Li, M. Zhou, X. Liu, H. Li, **H. Wang,** Y. Shen, M. Zhu, R. Jin*. "Ultrabright $Au@Cu_{14}$ Nanoclusters: 71.3% Phosphorescence Quantum Yield in Non-degassed Solution at Room Tempe rature" submi tted, **2020.**
2. C. Fei, M. Zhou, **H. Wang*.** " Manipul ating the Growth of DMAPbh for Efficient and Stable CsPbh Solar Cells" in preparation, **2020.**

e) any inte raction s with industry or with Air Force Research Laboratory scientists or significant collaborations that resulted from this work.

1. Prof. Luisa Whittaker-Brooks at University of Utah (PI in AFOSR organic materials chemistry program)
2. Prof. Zhibin Yu at Florida State University (Pl in AFOSR organic materials chemistry program)

All the published papers and manuscripts not yet published are available. Since the length is long, they are not attached here.

DD882 and SF425 are attached at the end of this file.

Reference:

1. Green, M.A.; Ho-Baillie, A.; Snaith, H.J., The Emergence of Perovskite Solar Cells. *Nat. Photonics* **2014,** *8,* 506.
2. Luo, S.; Daoud, W. A., Recent Progress in Organic-Inorganic Halide Perovskite Solar Cells: Mechanisms and Material Design. *J Mater. Chem. A* **2015,** *3,* 8992.
3. Sum, T. C.; Mathews, N., Advancements in Perovskite Solar Cells: Photophysics Behind the Photovoltaics. *Energy Environ. Sci.* **2014,** 7, 2518.
4. Lin, Q.; Armin, A.; Nagiri, R. C. R.; Burn, P. L.; Meredith, P., Electro-Optics of Perovskite Solar Cells. *Nat. Photonics* **2015,** *9,* 106.
5. D'Innocenzo, V.; Grancini, G.; Alcocer, M. J.P.; Kandada, A. R. S.; Stranks, S. D.; Lee, M. M.; Lanzani, G.; Snaith, H. J.; Petrozza, A., Excitons Versus Free Charges in Organo-Lead Tri-Halide Perovskites. *Nat. Commun.* **2014,** *5,* 3586.
6. Frost, J.M.; Butler, K. T.; Brivio, F.; Hendon, C.H.; van Schilfgaarde, M.; Walsh, A., Atomistic Origins of High-Performance in Hybrid Halide Perovskite Solar Cells. *Nano Lett.* **2014,** *14,* 2584.
7. Oga, H.; Saeki, A.; Ogomi, Y.; Hayase, S.; Seki, S., Improved Understanding of the Electronic and Energetic Landscapes of Perovskite Solar Cells: High Local Charge Carrier Mobility, Reduced Recombination, and Extremely Shallow Traps. *J Am. Chem. Soc.* **2014,** *136,* 13818.
8. Wehrenfennig, C.; Eperon, G. E.; Johnston, M. B.; Snaith, H. J.; Herz, L. M., High Charge Carrier Mobilities and Lifetimes in Organolead Trihalide Perovskites. *Adv. Mater.* **2014,** *26,* 1584.
9. Wehrenfennig, C.; Liu, M.; Snaith, H. J.; Johnston, M. B.; Herz, L. M., Charge-Carrier Dynamics in Vapour-Deposited Films of the Organolead Halide Perovskite CH3NH3Pbh-xClx. *Energy Environ. Sci.* **2014,** 7, 2269.
10. Ponseca Jr, C. S.; Savenije, T. J.; Abdellah, M.; Zheng, K.; Yartsev, A.; Pascher, T.; Harlang, T.; Chabera, P.; Pullerits, T.; Stepanov, A.; Wolf , J.-P.; Sundstrom, V., Organometal Halide Perovskite Solar Cell Materials Rationalized: Ultrafast Charge Generation, High and Microsecond-Long Balanced Mobilities, and Slow Recombination. *J Am. Chem. Soc.* **2014,** *136,* 5189.
11. Stranks, S. D.; Eperon, G. E.; Grancini, G.; Menelaou, C.; Alcocer, M. J. P.; Leijtens, T.; Herz, L. M.; Petrozza, A.; Snaith, H. J., Electron-Hole Diffusion Lengths Exceeding 1 Micrometer in an Organometal Trihalide Perovskite Absorber. *Science* **2013,** *342,* 341.
12. Manser, J. S.; Kamat, P. V., Band Filling with Free Charge Carriers in Organometal Halide Perovskites. *Nat. Photonics* **2014,** *8,* 737.
13. Stamplecoskie, K. G.; Manser , J. S.; Kamat, P. V., Dual Nature of the Excited State in Organic-Inorganic Lead Halide Perovskites. *Energy Environ. Sci.* **2015,** *8,* 208.
14. Xing, G.; Mathews, N.; Sun, S.; Lim, S.S.; Lam, Y. M.; Gratzel, M.; Mhaisalkar, S.; Sum, T. C., Long-Range Balanced Electron- and Hole-Transport Lengths in Organic-Inorganic CH3NH3P bl). *Science* **2013,** *342,344.*
15. Zhou, M.; Fei, C.; Sarmiento , J. S.; Wang, H., Manipulating the Phase Distributions and Carrier Transfers in Hybrid Quasi-Two-Dimensional Perovskite Films. *Solar RRL* **2019,** *3,* 1800359.
16. Fei, C.; Zhou, M.; Ogle, J.; Smilgies, D.-M.; Whittaker-Brooks, L.; Wang, H., Self-assembled propylammonium cations at grain boundaries and the film surface to improve the efficiency and stability of perovskite solar cells. *J Mater. Chem. A* **2019,** 7, 23739.
17. Fei, C.; Wang, H., Age-induced recrystallization in perovskite solar cells. *Org. Electron.* **2019,** *68,* 143.

18. Zhou, M.; Sarm iento, J. S.; Fei, C.; Zhang, X.; Wang, H., Effect of Composition on the Spin Relaxation of Lead Halide Perovskites. *J. Phys. Chem. Lett.* **2020,** *11*, 1502.
19. Zhou, M.; Sarmiento, J. S.; Fei, C.; Wang, H., Charge Transfer and Diffusion at the Perovsk ite /P CBM Interface Probed by Transient Absorption and Reflection. *J. Phys. Chem.* C **2019,** *123*, 22095.
20. Fei, C.; Sarmien to, J. S.; Wang, H., Generation of Coherent Optical Phonons in Methylammonium Lead Iodide Thin Films. *J. Phys. Chem.* C **2018,** *122*, 17035.
21. Shan, X.; Zhang, S.; Zhou, M.; Geske, T.; Davis , M.; Hao, A.; Wang, H.; Yu, Z., Porous Halide Perovskite-Polymer Nanocomposites for Explosive Detection with a High Sensitivity. *Adv. Mater. Interfaces* **2019,** *6*, 1801686.
22. Li, Y.; Cowan, M. J.; Zhou, M.; Taylor, M. G.; Wang, H.; Song, Y.; Mpourmpakis , G.; Jin , R., Heterometal-Doped M23 (M = Au/Ag/Cd) Nanoclusters with Large Dipole Moments. *ACS Nano* **2020,** *14*, 6599.
23. Li, J.; Lu, J. ; Chew, A.; Han, S.; Li, J.; Wu, Y.; Wang , H.; Ghimire, S.; Chang, Z. Attosecond science based on high harmonic generation from gases and solids. *Nat. Com mun.* **2020,** *II* , 2748.
24. Titze, M.; Fei, C.; Muno z, M.; Wang, X.; Wang, H.; Li, H. , Ultrafast Carrier Dynamics of Dual Emissions from the Orthorhombic Phase in Methylammoni um Lead Iodide Perovskites Revealed by Two-Dimensional Coherent Spectroscopy. *J. Phys. Chem. Lett.* 2019, 10, 4625.
25. Fei, C.; Guo , L. ; Li, B.; Zhang, R.; Fu, H. ; T ian, J. ; Cao, G., Controlled growth of textured perovskite films towards high performance solar cells. *Nano Energy* **2016,** *27*, 17.
26. Cheng, P.; Xu, Z.; Li, J.; Liu, Y.; Fan, Y.; Yu, L.; Smilgies, D.- M.; M üller, C.; Zhao, K.; Liu , S. F., Highly Efficient Ruddlesden-Popper Halide Perovskite PA2 MA4Pb5116 Solar Cells. *ACS Energy Lett.* **2018,** *3*, 1975.
27. Soe, C. M. M.; Nie , W.; Stoumpos , C. C.; Tsai, H.; Blancon, J.- C.; Liu, F.; Even, J.; Marks, T. J.; Mohite, A. D.; Kanatzid is , M. G., Understanding Film Fo rma tion Morphology and Orientation in High Member 2D Ruddlesden-Popper Perovskite s for High-Efficiency Solar Cells. *Adv. Energy Mater.* **2018,** *8*, 1700979.
28. Yang, Y.; Yang, M.; Moore, David T.; Yan, Y.; Mi lle r, Elisa M.; Zhu, K.; Beard, Matthew C., Top and bottom surfaces limit carrier lifetime in lead iodide perovskite fi lms. *Nat. Energy* **2017,** *2*, 16207.
29. Niu, G.; Yu, H. ; Li, J.; Wang, D.; Wang , L., Contrailed Orientation of Perovskite Films through Mixed Cations toward High Performance Perovs ite Solar Cells. *Nano Energy* **2016,** *27*, 87.
30. Hu, L.; Sun, K.; Wang, M.; Chen, W.; Yang, B.; Fu , J. ; Xio ng, Z.; Li, X.; Tang, X.; Zang, Z.; Zhang, S.; Sun , L.; Li, M., Inverted Planar Pero vskite Solar Cells with a High Fill Factor and Negligible Hysteresis by the Dual Effect of N aCl-D oped PEDOT:PSS. *ACS Appl. Mater. Interfaces* **2017,** *9*, 43902.
31. Chiang, C. H.; Wu, C. G., Film Grain-Size R elat

P-CsPbB-based perovskite solar cells with effic ie nc ies > 18%. *Science* **2019,** *365* , 591.
35. Even, J.; Pedesseau , L.; Jancu, J.-M.; Katan, C., Importance of Spin-Orbit Coupling in Hybrid Organic /Inorganic Perovskites for Photovoltaic Applications. *J Phys. Chem. Lett.* **2013,** *4,* 2999.
36. Im, J.; Stoumpos , C. C.; Jin, H.; Freeman, A. J.; Kanatzidis, M. G., Antagonism between Spin-Orbit Coupling and Steric Effects Causes Anomalous Band Gap Evolution in the Perovskite Photovoltaic Materials CH3NH3Sn1 - xP bxh*J Phys . Chem. Lett.* **2015,** *6,* 3503.
37. Kepenekian, M.; Even, J., Rashba and Dresselhaus Couplings in Halide Perovskites: Accomplishments and Opportunities for Spintronics and Spin-Orbitronics. *J Phys. Chem. Lett.* **2017,** *8,* 3362.
38. Ping, Y.; Zhang, J. Z., Spin-optotronic Properties of Organometal Halide Perovskites. *J Phys. Chem. Lett.* **2018,** *9,* 6103.
39. Yang, Y.; Feng, S.; Li, Z.; Li, T.; Xiong, Y.; Cao, L.; Gao, X., Unexpected Outstanding Room Temperature Spin Transport Verified in Organic-Inorganic Hybrid Perovskite Film. *J Phys. Chem. Lett.* **2019,** *10,* 4422.
40. Belykh, V. V.; Yakovlev , D. R.; Glazov, M. M.; Grigoryev, P. S.; Hussain, M.; Rautert, J.; Dirin, D. N.; Kovalenko , M. V.; Bayer, M., Coherent spin dynamics of electrons and holes in CsPbBr3 perovskite crystals. *Nat. Commun.* **2019,** *JO ,* 673.
41. Frohna, K.; Deshpande, T.; Harter, J.; Peng, W.; Barker, B. A.; Neaton, J.B.; Louie , S. G.; Bakr, 0. M.; Hsieh, D.; Bernardi, M., Inversion symmetry and bulk Rashba effect in methylammonium lead iodide perovskite single crystals. *Nat. Commun.* **2018,** *9,* 1829.
42. Wang, J.; Zhang, C.; Liu, H.; McLaughl in, R.; Zhai, Y.; Vardeny , S. R.; Liu , X.; McGill, S.; Semenov, D.; Guo , H.; Tsuchikawa, R.; Deshpande, V. V.; Sun, D.; Vardeny , Z. V., Spin-optoelectronic devices based on hybrid organic-inorganic trihalide perovskites. *Nat. Commun.* **2019,** *JO* , 129.
43. Gio vann i, D.; Lim, J. W. M.; Yuan, Z.; Lim , S. S.; Righe tto, M.; Qin g, J.; Zhang, Q.; Dewi, H. A.; Gao, F.; Mhaisalkar, S. G.; Mathews, N.; Sum, T. C., Ultrafast long-range spin-funneling in solution-processed Ruddlesden-Popper halide perovskites. *Nat. Commun.* **2019,** *10,* 3456.
44. Awschalo m, D. D.; Platte, M. E., Challenges for semiconductor spintronics. *Nat. Phys.* **2007,** *3,* 153.
45. Zutic, I.; Fabian, J.; Das Sarma, S., Spintronics: Fundamentals and applications. *Rev. Mod. Phys.* **2004,** *76,* 323.
46. Giov anni, D. ; Ma, H.; Chua, J.; Gratzel, M.; Ramesh, R. ; Mhais alkar, S.; Mathews, N.; Sum, T. C., Highly Spin-Polarized Carrier Dynamics and Ultralarge Photoinduced Magnetization in CH3NH3Pbb Perovskite Thin Films. *Nano Lett.* **2015,** *15,* 1553.
47. Odenthal, P.; Talmadge, W.; Gundlach, N.; Wang, R.; Zhang, C.; Sun , D.; Yu, Z.-G.; Valy Vardeny , Z.; Li, Y. S., Spin-polarized exciton quantum beating in hybrid organic-inorganic perovskites. *Nat. Phys.* **2017,** *13* , 894.
48. Gio vanni, D.; Chong, W. K.; Liu, Y. Y. F.; Dewi, H. A.; Yin, T.; Lekina, Y.; Shen, Z. X.; Mathews , N.; Gan, C. K.; Sum, T. C., Coherent Spin and Quasiparticle Dynamics in Solution-Processed Layered 2D Lead Halide Perovskites. *Adv. Sci.* **2018,** *5,* 1800664.
49. Kim , M.; Im, J.; Freeman, A. J.; Ihm, J.; Jin, H. , Switchable S= 1/2 and J= 1/2 Rashba bands in ferroelectric halide perovskites. *Proc. Natl. Acad. Sci. U S.A.* **2014,** *111,* 6900.
50. Niesne r, D.; Wil helm, M.; Levchuk, I. ; Osvet , A.; Shrestha, S. ; Batentschuk, M.; Brabec, C.; Fauste r, T., Giant Rashba Splitting in $CH_3NH_3PbBr_3$ Organic-Inorganic Perovskite. *Phys. Rev. Lett.* **2016,** *117,* 126401.

51. Nies ner, D.; Hauck , M.; Shres tha, S.; Levchuk, I. ; Matt, G. J.; Osvet, A.; Batentschuk, M.; Brabec, C.; Weber, H. B.; Fauster , T., Structural fluctuations cause spin-split states in tetragonal (CH_3NH_3)P bl) as evidenced by the circular photogalvanic effect. *Proc. Natl. Acad. Sci. US.A.* **2018,** *115,* 9509.
52. Zheng, F.; Tan, L. Z.; Liu , S.; Rappe, A. M., Rashba Spin-Orbit Coupling Enhanced Carrier Lifetime in CH_3NH_3P bh. *Nano Lett.* **2015,** *15,* 7794.
53. Yin , J.; Maity, P.; Xu, L. ; El- Zohry, A. M.; Li, H.; Bakr, 0. M.; Bredas, J.-L.; Mohammed, 0. F., Layer-Dependent Rashba Band Splitting in 2D Hybrid Perovskites. *Chem. Mater.* **2018,** *30,* 8538.
54. Zhai, Y.; Baniy a, S.; Zhang, C.; Li, J. ; H aney, P.; Sheng, C.-X.; Ehrenfreund , E.; Vardeny, Z. V., Giant Rashba splitting in 2D organic-inorganic halide perovskites measured by transient spectroscopies. *Sci. Adv.* **2017,** *3,* el 700704.
55. Song, P. H.; Kim, K. W., Spin relaxation of conduction electrons in bulk III-V semiconductors. *Phy. Rev. B* **2002,** *66,* 035207.
56. Song, Y.; Dery, H. , Analysis of phonon-induced spin relaxation processes in silicon. *Phy. Rev. B* **2012,** *86,* 085201.
57. Cummin gs, A. W.; Roche, S., Effects of Dephasing on Spin Lifetime in Ballistic Spin-Orbit Materials. *Phys. Rev. Lett.* **2016,** *116,* 086602.
58. Elliott , R. J., Theory of the Effect of Spin-Orbit Coupling on Magnetic Resonance in Some Semiconductors. *Phy. Rev.* **1954,** *96,* 266.
59. Yafet, Y., *Solid State Physics.* Academic: New York, 1963; Vol. 14.
60. Dyakonov, M., Spin orientation of electrons associated with the interband absorption of light in semiconductors. *Sov. Phys. JETP* **1971,** *60,* 1053.
61. Bir, G.; Aronov, A.; Pikus, G., Spin relaxation of electrons due to scattering by holes . *Sov. Phys. JETP* **1975,** *42,* 705.
62. Guo, Z.; Wu, X.; Zhu, T.; Zhu, X.; Huang, L., Elec tron- Phonon Scattering in Atomically Thin 2D Perovskites. *ACS Nano* **2016,** *I 0,* 9992.
63. Chen, X.; Lu, H.; Li, Z.; Zhai, Y.; Ndione, P. F.; Berry, J. J.; Zhu, K. ; Yang, Y.; Beard, M. C., Impact of Layer Thickness on the Charge Carrier and Spin Coherence Lifetime in Two-Dimen sional Layered Perovskite Single Crystals. *ACS Energy Lett.* **2018,** *3,* 2273.
64. Correa-Baena, J.-P.; Abate , A.; Sali ba, M.; Tress, W.; Jesper Jacobsson, T.; Griitzel, M.; Hagfeldt, A., The rapid evolution of highly efficient perovskite solar cells. *Energy Environ. Sci.* **2017,** *JO,* 710.
65. Zhou, H.; Chen , Q.; Li, G.; Luo , S.; Song, T.-b.; Duan, H.-S.; Hong, Z.; You, J.; Liu , Y.; Yang, Y., Interface engineering of highly efficient perovskite solar cells. *Science* **2014,** *345, 542.*
66. Gharibzadeh, S.; Valduga de Almeida Camargo, F.; Roldan-Carmona , C.; Gschwend, G. C.; Pascual , J. ; Tena- Zaera, R.; Cerullo, G.; Grancini , G.; Nazeeruddin , M. K., Picosecond Capture of Photoexcited Electrons Improves Photovoltaic Conversion m MAPbl3:C70-Doped Planar and Mesoporous Solar Cells. *Adv. Mater.* **2018,** *30,* 1801496.
67. Ponseca, C. S.; Hutter , E. M.; Piatkowski, P. ; Cohen , B.; Pascher , T.; Douhal, A.; Yartsev, A.; Sundstrom, V.; Savenije , T. J., Mechanism of Charge Transfer and Recombination Dynamics in Organo Metal Halide Perovskites and Organic Electrodes, PCBM, and Spiro-OMeTAD: Role of Dark Carriers. *J Am. Chem. Soc.* **2015,** *137,* 16043.
68. Hutter, E. M.; Hofman, J.-J.; Petrus, M. L.; Moes, M.; Abell6n, R. D. ; Docampo , P.; Savenije , T. J., Charge Transfer from Methylammonium Lead Iodide Perovskite to Organic Transport Materials: Efficienc ies , Transfer Rates, and Interfacial Recombination. *Adv. Energy Mater.* **2017,** 7, 1602349.

69. Ponseca, C. S.; Savenije, T. J.; Abdellah, M.; Zheng, K.; Yartsev, A.; Pascher , T.; Harla ng, T.; Chabera, P.; Pullerits, T.; Stepanov, A.; Wolf, J.-P .; Sunds trom, V., Organometal Halide Perovskite Solar Cell Materials Rationalized: Ultrafast Charge Generatio n, High and Microsecond-Long Balanced Mobil ities , and Slow Recombination. *J Am. Chem. Soc*. **2014,** *136,* 5189.
70. March io ro, A.; Teuscher , J.; Frie drich , D.; Kuns t, M.; van de Krol, R.; Moehl, T.; Gratzel, M.; Moser, J.-E., Unravelling the mechanism of photoinduced charge transfer processes in lead iodide perovskite solar cells. *Nat. Photonics* **2014,** *8,* 250.
71. Xin g, G.; Wu, B.; Chen, S.; Chua, J.; Yanta ra, N.; Mhaisalkar , S.; Mathews, N.; Sum, T. C., Interfacial Electron Transfer Barrier at Compact TiO2/CH3NH3Pbl3 Heterojunction. *Small* **2015,** *11,* 3606.
72. Piatkowsk i, P.; Cohen, B.; Javier Ramos, F.; Di Nunzio , M.; Nazeerudd in , M. K.; Gratzel, M.; Ahmad, S.; Douhal, A., Direct monitoring of ultrafast electron and hole dynamics in perovskite solar cells. *Phys. Chem. Chem. Phys.* **2015,** *17,* 14674.
73. Wang, L.; McCleese , C.; Kovalsky, A.; Zhao, Y.; Burd a, C., Femtosecond Time-Resolved Transient Absorption Spectroscopy of CH3NH3Pbl3 Perovskite Films: Evidence for Passivation Effect of Pbl2. *J Am. Chem. Soc.* **2014,** *136,* 12205.
74. Pydzinsk a-Bia!ek, K.; Szeremeta, J.; Wojc iec howski , K.; Zi6lek, M., Insights into the Femtosecond to Nanosecond Charge Carrier Kinetics in Perovskite Materials for Solar Cells. *J Phys. Chem. C* **2019,** *123,* 110.
75. Horn, J.; Minda, I.; Schwoerer, H.; Schlettwein, D., Direct Observation of Charge Injection From CH3NH3Pbl3-xClx to Organic Semiconductors Monitored With sub-ps Transient Absorption Spectroscopy. *Phys. Status Solidi B.* **2019,** *256* , 1800265.
76. Dursun , I.; Mait y, P.; Yin, J.; Turedi, B.; Zhumekenov , A. A.; Lee, K. J.; Mohammed, 0. F.; Bakr, 0. M., Why are Hot Holes Easier to Extract than Hot Electrons from Methylammonium Lead Iodide Perovskite? *Adv. Energy Mater.* **2019,** *9,* 1900084.
77. Kim, J.; Godin, R.; Dimitrov, S. D.; Du, T.; Bryant, D.; McLachla n, M.A.; Durrant, J. R., Excitation Density Dependent Photoluminescence Quenching and Charge Transfer Efficiencies in Hybrid Perovskite/Organic Semiconductor Bilayers. *Adv. Energy Mater.* **2018,** *8,* 1802474.
78. Pydzinska, K.; Karo lc zak, J.; Kosta , I.; Tena-Zaera, R.; Tod inova, A.; Idigoras, J.; Anta, J. A.; Zi6lek, M., Determination of Interfacial Charge-Transfer Rate Constants in Perovskite Solar Cells. *ChemSusChem* **2016,** *9,* 1647.
79. Leng, J.; Liu, J. ; Zhang, J.; Jin, S., Decoupling Interfacial Charge Transfer from Bulk Diffusion Unravels Its Intrinsic Role for Efficient Charge Extraction in Perovskite Solar Cells. *J Phys. Chem. Lett.* **2016,** 7, 5056.
80. Yang, Y.; Yang, M.; Li, Z.; Cris p, R.; Zhu, K.; Beard, M. C., Comparison of Recombination Dynamics in CH3NH3PbBr3 and CH3NH3Pbl3 Perovskite Films: Influence of Exciton Binding Energy. *J Phys. Chem. Lett.* **2015,** *6,* 4688.
81. Yang, Y.; Ostrowski, D. P.; France, R. M.; Zhu, K.; van de Lagemaat, J.; Luther, J. M.; Beard, M. C., Observation of a hot-phonon bottleneck in lead-iodide perovskites. *Nat. Photonics* **2015,** *10,* 53.
82. Zhu, H .; T rinh , M. T.; Wang, J.; Fu, Y.; Joshi, P. P. ; Miyata, K.; Jin, S.; Zhu, X.-Y., Organic Cations Might Not Be Essentia l to the Remarkable Properties of Band Edge Carriers in Lead Halide Perovskites. *Adv. Mater.* **2017,** *29,* 1603072.